

## Article

## Structural Arrangement and Computational Exploration of Guanidinium Based Ionic Liquids with Benzoic Acid Derivatives as Anion

V. Ramkumar, Indrajit Das, and Ramesh L. Gardas

*Cryst. Growth Des.*, **Just Accepted Manuscript** • Publication Date (Web): 26 Mar 2019

Downloaded from <http://pubs.acs.org> on March 27, 2019

### Just Accepted

“Just Accepted” manuscripts have been peer-reviewed and accepted for publication. They are posted online prior to technical editing, formatting for publication and author proofing. The American Chemical Society provides “Just Accepted” as a service to the research community to expedite the dissemination of scientific material as soon as possible after acceptance. “Just Accepted” manuscripts appear in full in PDF format accompanied by an HTML abstract. “Just Accepted” manuscripts have been fully peer reviewed, but should not be considered the official version of record. They are citable by the Digital Object Identifier (DOI®). “Just Accepted” is an optional service offered to authors. Therefore, the “Just Accepted” Web site may not include all articles that will be published in the journal. After a manuscript is technically edited and formatted, it will be removed from the “Just Accepted” Web site and published as an ASAP article. Note that technical editing may introduce minor changes to the manuscript text and/or graphics which could affect content, and all legal disclaimers and ethical guidelines that apply to the journal pertain. ACS cannot be held responsible for errors or consequences arising from the use of information contained in these “Just Accepted” manuscripts.



1  
2  
3 **Structural Arrangement and Computational Exploration of Guanidinium**  
4 **Based Ionic Liquids with Benzoic Acid Derivatives as Anion**  
5  
6

7  
8 V. Ramkumar, Indrajit Das and Ramesh L. Gardas\*  
9

10 Department of Chemistry, Indian Institute of Technology Madras, Chennai – 600036, India  
11

12 \*Corresponding author: *e-mail address: [gardas@iitm.ac.in](mailto:gardas@iitm.ac.in)*  
13

14 *URL: <http://www.iitm.ac.in/info/fac/gardas>*

15 *Tel.: +91 44 2257 4248; Fax: +91 44 2257 4202*  
16  
17  
18  
19  
20  
21  
22  
23  
24  
25  
26  
27  
28  
29  
30  
31  
32  
33  
34  
35  
36  
37  
38  
39  
40  
41  
42  
43  
44  
45  
46  
47  
48  
49  
50  
51  
52  
53  
54  
55  
56  
57  
58  
59  
60

## Abstract

Crystallisation of ionic liquids [ILs], is of great interest for determining the crystal structure and molecular interactions. Hydrogen bonding is an important non-covalent interaction, which is related to the properties of ILs. In this context, we have prepared 1,1,3,3-tetramethylguanidine [TMG] based ionic liquids (ILs), with different benzoic acid derivatives as anions and the crystal structure of these ILs were determined at low temperature (173(2) K) to understand the interactions and their network formation. Using Hirshfeld surface analysis the intermolecular interactions in crystal packing of ILs were analyzed and quantified. Density functional theory (DFT) calculation was done to ascribe the thermodynamic properties of these ILs. Molecular geometry of the guanidinium ionic liquids was optimized and the electronic properties and HOMO and LUMO energies were calculated using the DFT at B3LYP/6-311G++(d,p) level. The characterization of the ILs was done by TGA, DSC, NMR and IR.

## 1. Introduction

Ionic liquids (ILs) are green solvents possess fascinating physical properties and provide good opportunity to industrialists furnishing alternative solvents, which are environmental friendly<sup>1-2</sup>. They generally exist as anions and cations in the liquid-state. The importance of hydrogen bonding in ILs is a subject of debate for several decades and there is a general view that ILs are dominated by Coulombic interactions. Determination of the type of interaction, be it Coulombic interaction, dispersive forces, hydrogen bonding, is the need of the hour<sup>3</sup>. Seddon *et al.* first reported the presence of hydrogen bonding in imidazolium salts<sup>4</sup>. Later, the presence of hydrogen bonded ion-ion interaction in molten salt was studied by Dymek *et al.*<sup>5</sup> and several studies were done using techniques like NMR, X-Ray diffraction, IR<sup>6</sup> and theoretical studies<sup>7</sup> to substantiate the presence of hydrogen bonding in ILs .

Hydrogen bonding interaction in ILs is considered crucial for the evaluation of ILs structure and it is the most important interaction in molecular crystals. This also distinguishes protic ILs from other ILs, which form the proton-donor-acceptor sites and the network structure. The attractive interaction between a hydrogen atom from a molecule or a molecular fragment and an atom or a group of atoms in the same or different molecule, which provide evidence for the bond formation is referred to as hydrogen bonding<sup>8</sup>. Hydrogen bonding is formed during the synthesis as an ion transfer and this is a trade mark of ILs<sup>9</sup>. For understanding the modes of interaction and

1  
2  
3 conformational influence of cations and anions on the lattice energies, melting points and general  
4 behavior of ILs, the determination of hydrogen-bonding environments is critical<sup>10</sup>. A careful  
5 selection of anion and cation is essential as they influence the molecular structure and packing  
6 resulting in several distinct conformations<sup>11</sup>. Anions of different size, symmetry and hydrogen  
7 bonding capability are chosen to study the effect of the anion on crystalline behavior<sup>12</sup>. Ralf  
8 Ludwig *et al.*<sup>13,6</sup> have used X-ray diffraction tool to determine the existence of H-bonding between  
9 anion and cation, which is a strong evidence in both solid and liquid states.

10  
11  
12 1,1,3,3-tetramethylguanidinium [TMG] based ILs have wide applications such as SO<sub>2</sub>  
13 capture<sup>14,15,16,17</sup>, production of biofuels<sup>18</sup>, synthesis of biolubricants<sup>19</sup>, as catalysts for aldol  
14 reaction<sup>20</sup> and as a medium for Mannich reactions<sup>21</sup>. The gas solubility<sup>22</sup> with efficient and  
15 reversible CO<sub>2</sub> capture through [TMG] based ILs was studied by Lei *et al.*<sup>23</sup>.

16  
17  
18 The X-ray crystal structure of ILs is difficult to study, as they are in the liquid state at room  
19 temperature and it is a challenging task to crystallize them<sup>24</sup>. A modern day technique is used now-  
20 a-days for structure determination of compounds with low melting points by *in situ* crystallisation  
21 using optical heating and crystallization device (OHCD)<sup>25</sup>. Winterton *et al.*<sup>26</sup> have studied  
22 imidazolium based ILs by *in situ* cryo-crystallisation method using OHCD. Deepak *et al.*  
23 demonstrated the fact, that nature of intra and intermolecular interactions, which evolve on  
24 crystallizing liquids are similar to those observed in the solid-state<sup>27</sup>. TMG based ILs are rare and  
25 very few studies on crystal structures of [TMG]Cl<sup>28</sup>, [TMG]Br<sup>29</sup>, [TMG][Ac]<sup>30</sup>, [TMG][IM]<sup>23</sup>,  
26 [TMG][NTf<sub>2</sub>]<sup>31</sup>, [TMG][H<sub>2</sub>PO<sub>4</sub>]<sup>32</sup> and [TMG][NO<sub>3</sub>]<sup>33</sup> have been reported. Unlike other ILs, only  
27 less work on the study of cation-anion interaction has been done for TMG based ILs but recently  
28 a detailed comparison of thermophysical properties of [TMG][BEN] and [TMG][SAL] in the  
29 presence of water has been reported by Akhil *et al.*<sup>34</sup>. Carboxylic acid molecules, which usually  
30 form cyclic hydrogen-bonded dimers, are a commonly observed motif in the solid-state and  
31 derivatives of benzoic acid were used for this purpose as anions to study the intermolecular  
32 interactions and network formation.

33  
34  
35  
36  
37  
38  
39  
40  
41  
42  
43  
44  
45  
46  
47  
48  
49 Theoretical calculations are one way of accessing the fundamental nature of H-bonding in ILs,  
50 providing information through electronic structure on the geometry and vibrational spectra<sup>7</sup>.  
51 Studies to investigate H-bonding interactions in imidazolium based ILs by theoretical method  
52 confirmed that C–H... H-bonds existed between cations and anions<sup>35</sup>. H-bonds in imidazolium-  
53 based ILs perturb the Coulombic forces to deviate from charge symmetry and significantly  
54  
55  
56  
57  
58  
59  
60

influence the physicochemical properties due to cation.<sup>10</sup> The H-bonding through C-H and N-H bonds of the cations has significant influence on melting points, viscosities and enthalpy of vaporization in some ILs<sup>35</sup>.

Thermal studies also reveal the stability and interaction of H-bonding in ILs, which govern the important properties like glass transition temperature ( $T_g$ ), melting point ( $T_m$ ), boiling-point ( $T_b$ ), viscosity and ionicity of the ILs. By modifying the interaction between the cation and anion, the  $T_g$  values can be controlled<sup>36</sup>. It is also observed that the thermal behavior of salts strongly depends on the anion and its shape<sup>12</sup>.

Hirshfeld surface analysis for the ILs was performed to get an insight and quantify the intermolecular interactions in the crystal packing.

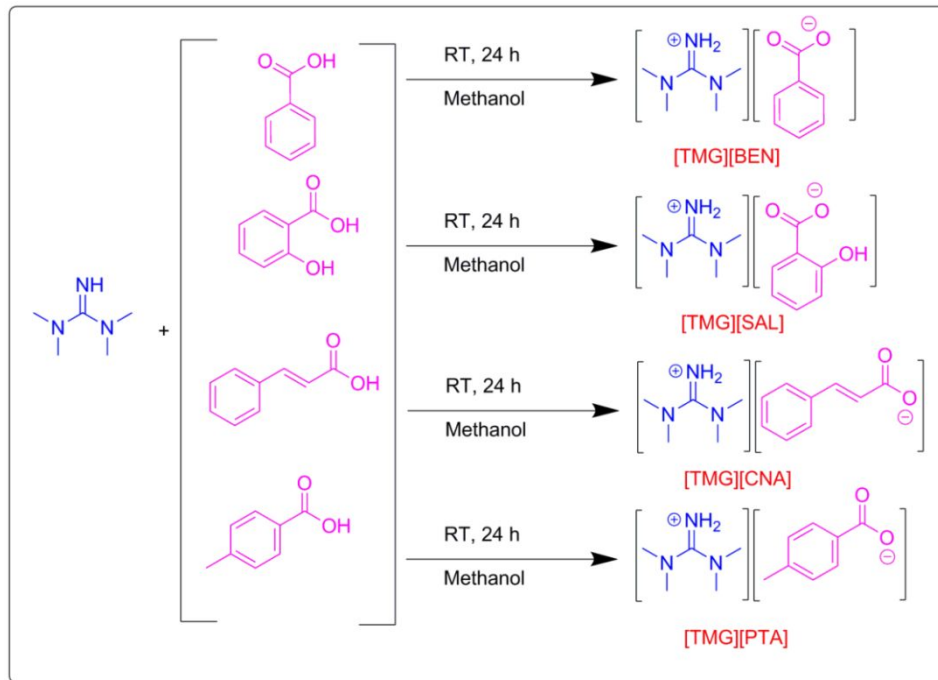
Hence, four TMG based ILs with different anions were synthesized and their hydrogen bonding and network arrangement were studied by single crystal XRD. Thermal studies and theoretical calculations with temperature dependence of the thermodynamic functions, HOMO-LUMO analysis to predict the charge transfer between the anion and cation, vibrational energy, and minimum energy studies using B3LYP calculations with 6-311++G(d,p) basis set were carried out.

## 2. Experimental Section

### 2.1 Synthesis and Characterization Data

The TMG unit is highly basic ( $pK_a=13.6$ )<sup>37</sup> and so it can be easily protonated in presence of any weak acid. We have synthesized four ILs by neutralization method using equimolar mixture of TMG (base) with different acids. TMG was added to equimolar amount of acids namely, benzoic acid, salicylic acid, cinnamic acid and para toluenic acid in the presence of methanol (scheme 1). The reaction was continuously stirred for 24 h under  $N_2$  atmosphere at room temperature. The excess solvent was removed by rotary evaporator and the product was dried under high vacuum for nearly 24 h under  $N_2$  atmosphere at room temperature. The ILs formed are tetramethylguanidinium benzoate [TMG][BEN], tetramethylguanidinium salicylate [TMG][SAL], (semi-solid in nature), tetramethylguanidinium cinnamate [TMG][CNA] and tetramethylguanidinium tolunate [TMG][PTA] (semi viscous in nature).

The obtained ILs were characterized by  $^1H$  NMR,  $^{13}C$  NMR, differential scanning calorimetry, thermogravimetric analysis and IR spectrophotometry.



**Scheme 1.** Synthesis of TMG based ILs with benzoic acid derivatives

$^1\text{H}$  NMR and  $^{13}\text{C}$  NMR spectra were recorded on a Bruker Avance-III spectrometer operating at 500 MHz with tetramethylsilane as the internal standard. The following abbreviations are used for the multiplicity of signals in  $^1\text{H}$  NMR: (s) singlet, (d) doublet, (t) triplet, (q) quartet, (m) multiplet. NMR spectra ( $\text{CDCl}_3$ , 25 °C) were recorded using Bruker Avance 500 MHz NMR spectrometer giving peak positions for the four ILs (Figures S1-S4).

**[TMG][BEN]:**  $^1\text{H}$  NMR (500 MHz)  $\delta$  (ppm): 2.87 (s, 12H,  $\text{CH}_3$ ), 4.85 (broad singlet, 2H,  $\text{NH}_2$ ), 7.29 (m, 3H, aromatic), 8.02 (d,  $J = 6.9$  Hz, 2H, aromatic).

$^{13}\text{C}$  NMR (125 MHz)  $\delta$  (ppm): 39.6 (N- $\text{CH}_3$ ), 127.6 (aromatic), 129.4 (aromatic), 129.6 (aromatic), 138.7 (aromatic), 162.3 ( $\text{COO}^-$ ), 172.6 (N=C).

**[TMG][SAL]:**  $^1\text{H}$  NMR (500 MHz)  $\delta$  (ppm): 2.93 (s, 12H,  $\text{CH}_3$ ), 6.75 (t,  $J = 7.15$  Hz, 1H, aromatic), 6.86 (d,  $J = 7.15$  Hz, 1H, aromatic), 7.26 (t,  $J = 7.47$  Hz, 1H, aromatic), 7.88 (d, 1H,  $J = 7.47$  Hz, aromatic), 8.75 (broad s, 2H, NH) 14.45 (s, 1H, OH)

$^{13}\text{C}$  NMR (125 MHz)  $\delta$  (ppm): 39.8 (N- $\text{CH}_3$ ), 116.4 (aromatic), 117.6 (aromatic), 119.7 (C-C=O, aromatic), 130.7 (aromatic), 132.5 (aromatic), 162.1 (C-OH), 162.4 ( $\text{COO}^-$ ), 174.5 (N=C).

1  
2  
3 [TMG][CNA] : <sup>1</sup>H NMR (500 MHz) δ (ppm): 2.95 (s, 12H, CH<sub>3</sub>), 3.47 (broad s, 2H, NH) 6.57  
4 (d, *J* = 15.6 Hz, 1H, olefin), 7.25 (t, *J* = 7.3 Hz, 1H, aromatic), 7.30 (t, *J* = 7.94 Hz, 2H, aromatic)  
5 7.4 (d, *J* = 15.6 Hz, 1H, olefin), 7.48(d, *J* = 7.94 Hz, 2H, aromatic).

6  
7  
8 <sup>13</sup>C NMR (125 MHz) δ (ppm): 39.8 (N-CH<sub>3</sub>), 116.5 (aromatic), 127.6 (aromatic), 128.4(C-C=O,  
9 aromatic), 128.6 (aromatic), 136.7 (aromatic), 138.5 (aromatic), 163.2 (C=O), 173.6 (N=C).

10  
11 [TMG][PTA]: <sup>1</sup>H NMR (500 MHz) δ (ppm): 2.33 (s, 3H, CH<sub>3</sub>), 2.90 (s, 12H, N-CH<sub>3</sub>), 4.90 (broad  
12 s 2H, NH), 7.10 (d, *J* = 7.90 Hz, 2H, aromatic), 7.91(d, *J* = 7.90 Hz, 2H, aromatic).

13  
14 <sup>13</sup>C NMR (125 MHz) δ (ppm): 21.5 (CH<sub>3</sub>), 39.70 (N-CH<sub>3</sub>), 128.3 (aromatic), 129.6 (aromatic),  
15 135.9 (aromatic), 139.70 (aromatic), 162.6 (C=O), 172.9 (N=C).

16  
17  
18 The water content of each ionic liquid after drying was determined by Karl Fisher titration method  
19 before measuring their thermophysical properties. The measurement was made with the help of  
20 Metrohm KF 870 Titrino in triplicates for each IL and the average values are presented in Table  
21 S1.  
22  
23  
24  
25

## 26 2.2 X-ray Diffraction Structure Determination

27  
28 The x-ray crystal structure was determined for all the TMG based ILs. Single-crystal X-ray  
29 structure data collection was performed on a Bruker AXS Kappa Apex II CCD diffractometer with  
30 graphite monochromated Mo K $\alpha$  radiation ( $\lambda = 0.71073 \text{ \AA}$ ). The ILs were taken in a vial and heated  
31 and cooled suddenly using liquid nitrogen and this process was repeated for several times till small  
32 crystals appeared. Crystal was picked carefully from the sides of the vial with a cryo-loop with a  
33 constant flow of liquid nitrogen. Cryo-loop was mounted onto the goniometer and the data were  
34 collected at 173 K. The unit cell determination was done with 32 frames at three different  
35 orientations of the detector to collect reflections and the program APEX2-S SAINT<sup>38</sup> was used for  
36 finding the unit cell parameters. The frames were integrated with the Bruker SAINT software  
37 package using a narrow-frame algorithm. The integration of the data was done to a maximum  $\theta$   
38 angle of 25.0°.  
39  
40  
41  
42  
43  
44  
45  
46

47  
48 The program SADABS was used for absorption correction using multi-scan procedure. The  
49 structures were solved by direct methods using SHELXTL software<sup>39</sup> and refined by full-matrix  
50 least squares techniques using SHELXT computer program<sup>39</sup>.  
51  
52  
53

54 All the hydrogens, except the nitrogen hydrogen were fixed at chemically meaningful positions  
55 and riding model refinement was applied. The hydrogen attached to the nitrogen was located  
56  
57  
58  
59  
60

through the difference Fourier map and refined with isotropic thermal parameters. The hydrogen atom bound to carbon atoms was constrained to a distance of C–H = 0.93–0.97 Å and  $U_{\text{iso}}(\text{H}) = 1.2U_{\text{eq}}(\text{C})$  and  $1.5U_{\text{eq}}(\text{C})$ . The hydrogen atom associated with the oxygen atom was allowed to ride on the parent atom with a distance of 0.82 Å and  $U_{\text{iso}}(\text{H}) = 1.5U_{\text{eq}}(\text{C})$ . Molecular graphics were drawn using ORTEP32<sup>40</sup> and Mercury programs<sup>41</sup>. The crystal data with refinement details are summarized in Table 1. The refinement of all the crystals was done using the data collected at low temperature with the help of kryoflex cooling system.

### 3. Result and Discussion

#### 3.1 Crystal Studies

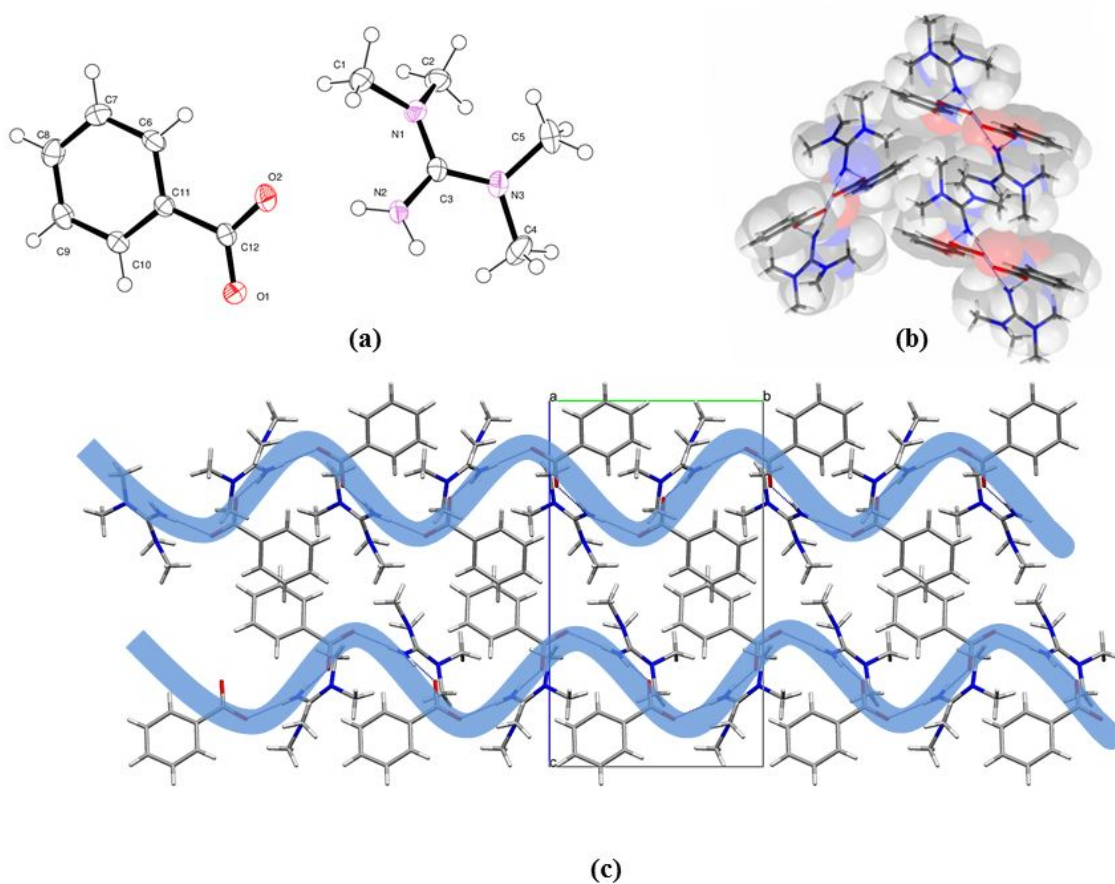
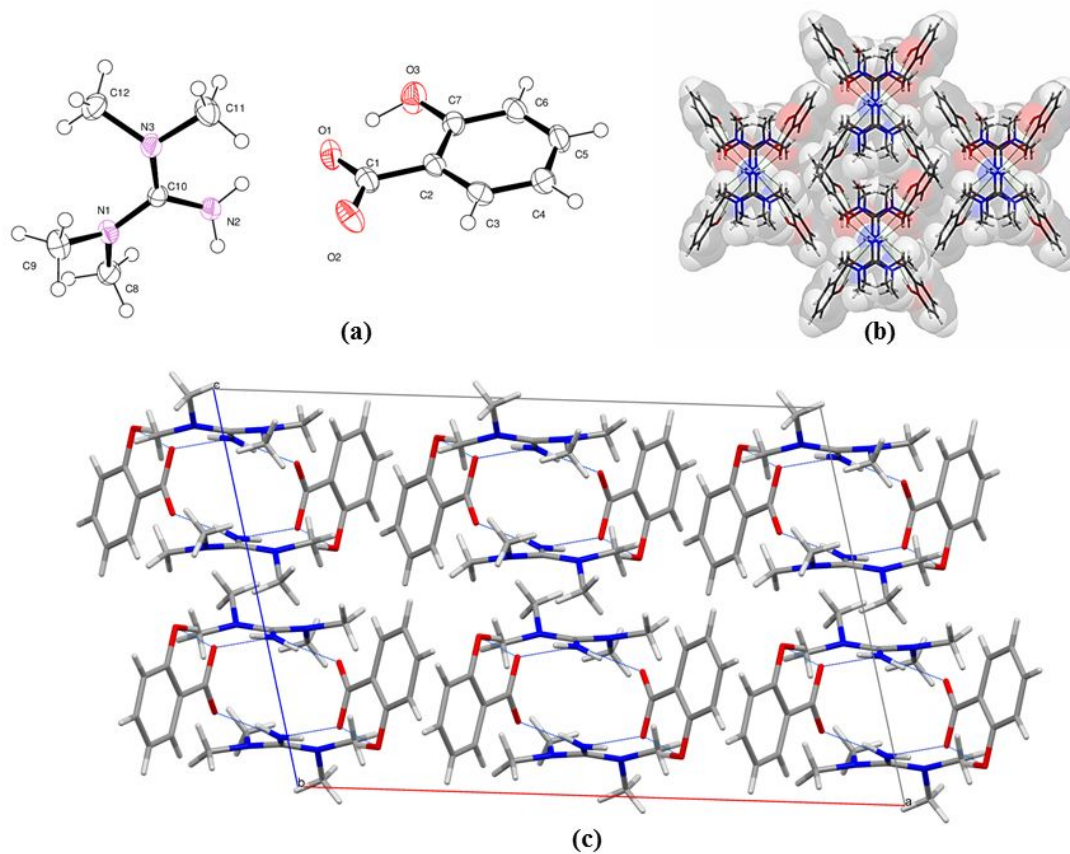


**Figure 1.** (a) ORTEP of [TMG][BEN] with 30% ellipsoid probability (b) N–H...O hydrogen bonding connected through  $C_2^2(6)$  chain motif (c) N–H...O interactions forming chains and wavelike pattern.

1  
2  
3 The structure of [TMG][BEN] was solved in the orthorhombic crystal system, space group  
4  $P2_12_12_1$ . The other three crystal structures were solved in the monoclinic crystal system, the space  
5 groups were  $C2/c$ ,  $P2_1/c$  and  $P2_1/c$  for [TMG][SAL], [TMG][CNA] and [TMG][PTA],  
6 respectively. The ORTEP<sup>40</sup> diagrams for the four ILs are drawn with 30% probability in Figure  
7 1a, 2a, 3a and 4a, respectively. In all the four ILs, the TMG core ( $N=C(N)_2$ ) shows a nearly ideal  
8 trigonal-planar geometry, as expected for  $sp^2$  hybridization and the anions benzoate,  
9 cinnamate and *para*-tolunate show a planar structure due to the presence of  $sp^2$  carbon atoms<sup>42</sup>. A  
10 similar [TMG] cation structure has already been reported by Berg *et. al.*<sup>31</sup> with [NTf<sub>2</sub>] as anion.  
11 An intramolecular hydrogen bonding C-H...O is seen particularly in [TMG][SAL] and N-H...O  
12 intermolecular hydrogen bonding is seen in all the four ILs. Generally the H...A (A = acceptor)  
13 distance of < 2.2 Å is described as strong hydrogen bonds.<sup>43</sup> The C-H...O and the N-H...O  
14 interaction distance and angles of the ILs show that the interactions are strong and they are  
15 hydrogen bonds in nature and are observed in all the four ILs.  
16  
17  
18  
19  
20  
21  
22  
23  
24  
25



53 **Figure 2.** (a) ORTEP of [TMG][SAL] with 30% ellipsoid probability (b) N-H...O hydrogen  
54 bond chains forming a “butterfly like pattern (c) N-H...O interactions along c-axis.  
55  
56  
57  
58  
59  
60

The two [TMG] cations are hydrogen-bonded to two anions related to each other by an inversion center in the case of [TMG][SAL], [TMG][PTA] and [TMG][CNA] giving rise to a network of molecules connected by hydrogen bonds in the form of a tetramer. The tetramer seems to be planar in the case of [TMG][PTA] and [TMG][CNA] but it is slightly folded like an ‘envelope’ in the case of [TMG][SAL] giving rise to a ‘butterfly like’ network pattern (Figure 2b).

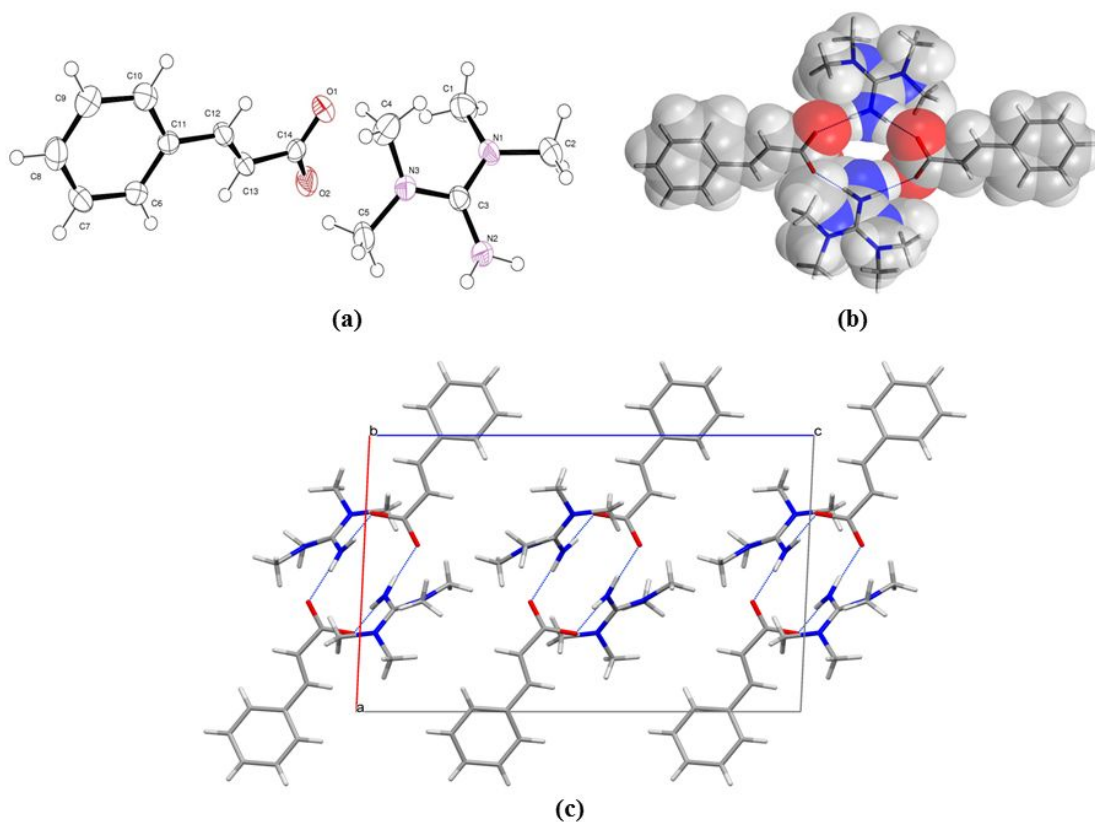


**Figure 3.** (a) ORTEP of [TMG][CNA] with 30% ellipsoid probability (b) N-H...O hydrogen bonding connected through  $R_4^4(12)$  ring motif (c) N-H...O interactions along c-axis.

The single crystal data of [TMG][BEN] clearly revealed that the cation was involved in hydrogen bonding interactions with two benzoate anions forming a chain  $C_2^2(6)$  graph set<sup>44</sup> interaction (Figure 2b). The  $\text{NH}_2$  group in [TMG] cation facilitates formation of hydrogen bond with the oxygens atoms of two anions. This forms hydrogen bonds with a distance of 1.91(2) Å and 1.93(2) Å (Table 2). N-H...O intermolecular hydrogen bond result in the formation of a “wavelike” pattern along the b-axis (Figure 1c). It is interesting to note that benzoic acid without TMG crystallises to

form a herringbone packing pattern by C-H... $\pi$  interactions forming a dimer<sup>45</sup>. The single crystal data of [TMG][SAL] showed that the cation was involved in hydrogen bonding interactions with two salicylate anions forming a ring type  $R_4^4(12)$  graph set interaction. The NH<sub>2</sub> group in [TMG] cation facilitates the formation of hydrogen bond with the oxygen atoms of two anions. This forms a hydrogen bond with a distance of 1.87(2) Å and 2.08(2) Å (Table 2). The network arrangements of the cation and the anion of the molecules along the c-axis is shown in Figure 2c.

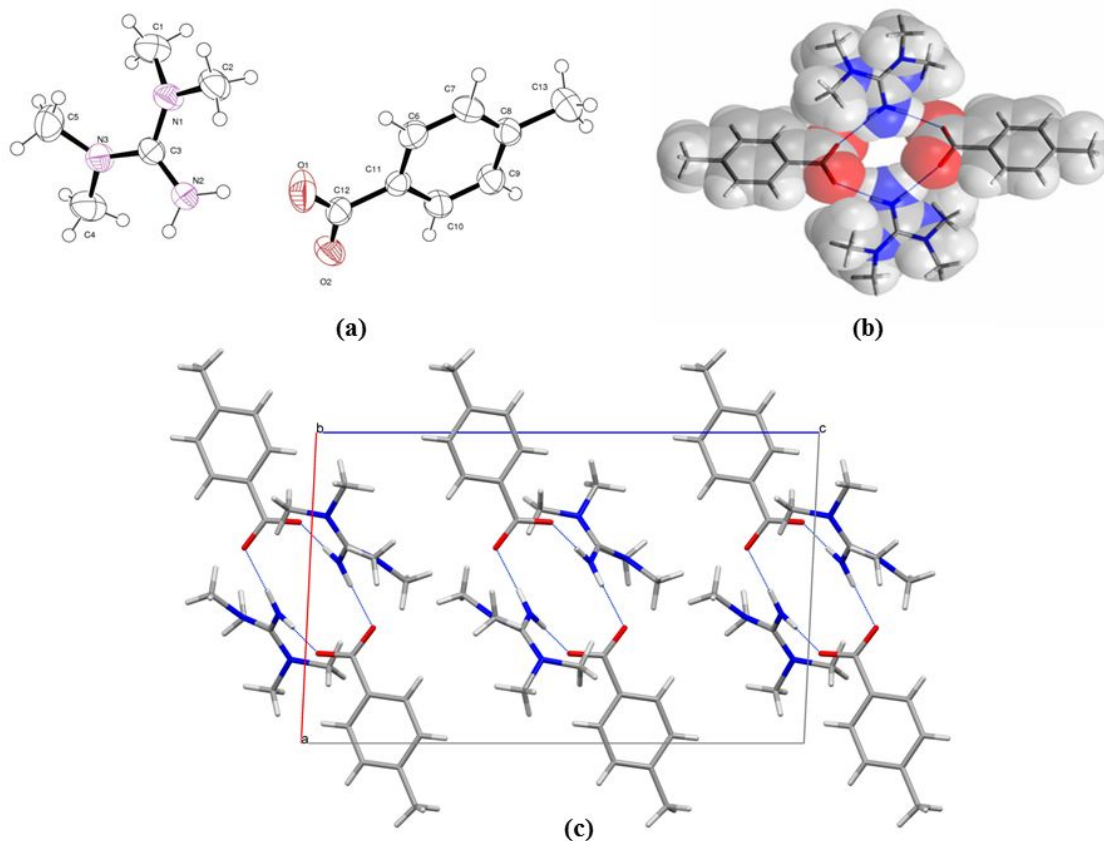


**Figure 4.** (a) ORTEP of [TMG][PTA] with 30% ellipsoid probability (b) N-H...O hydrogen bonding connected through  $R_4^4(12)$  ring motif (c) N-H...O interactions forming parallel shown along b-axis.

A similar ideal trigonal-planar arrangement of the cation core  $N=C(N)_2$  was also seen in [TMG][CNA]. The cinnamate anion phenyl ring shows a planar structure and the -COOH group linked to the -CH=CH- carbon atoms shows a slight deviation from the planarity. The torsion angle for the carbon atom attached to the -COOH group C12-C13-C14-O1 is  $-0.2(3)^\circ$  and for C12-C13-

1  
2  
3 C14-O2 is  $-175.8(2)^\circ$ . This deviation in the mean plane was due to the presence of  $-\text{CH}=\text{CH}-$   
4 group in the anion.  
5

6 The hydrogen bond interaction between the [TMG] cation and the two cinnamate anions is in the  
7 form of  $R_4^4(12)$  graph set interaction (Figure 3b). The  $\text{NH}_2$  group in [TMG] cation facilitates the  
8 formation of hydrogen bonds ( $\text{N-H}\cdots\text{O}$ ) with two oxygen atoms of cinnamate anion and the  
9 distances are  $1.91(3) \text{ \AA}$  and  $1.85(3) \text{ \AA}$  (Table 2). The packing diagram of the molecules along the  
10 b-axis is shown in Figure 3c.  
11  
12  
13  
14

15 Similar to [TMG][BEN], [TMG][SAL] and [TMG][CNA], trigonal-planar arrangement was  
16 observed in the  $\text{N}=\text{C}(\text{N})_2$  core of the [TMG][PTA]. The [TMG] cation in [TMG][PTA] has  $\text{N}-$   
17  $\text{H}\cdots\text{O}$  hydrogen bond interactions with two toluenate anions forming a  $R_4^4(12)$  graph set interaction  
18 (Figure 4b). The  $\text{NH}_2$  group in [TMG] cation facilitates the formation of hydrogen bonds with two  
19 oxygen atoms of the different anion and the distances are  $1.90(2) \text{ \AA}$  and  $1.93(2) \text{ \AA}$ . The network  
20 arrangement of cation and anion of the molecules along the b-axis is shown in Figure 4c.  
21  
22  
23  
24  
25  
26  
27

### 28 3. 2 Hirshfeld Surface analysis

29

30 The Hirshfeld surface is becoming a valuable tool for analysing intermolecular interactions while  
31 maintaining a whole-of-molecule approach. They can also be used in conjunction with a more  
32 direct atom...atom based approach to gain a fuller appreciation of the important interactions in a  
33 molecular crystal<sup>46</sup>. The molecular Hirshfeld surfaces reflect intermolecular interactions and the  
34 picture of molecular shape in a crystalline environment visually. The surface distances to the  
35 nearest atoms outside are represented as  $d_e$ , and inside as  $d_i$ , which are well defined and from these  
36 properties it is easy to explore the type as well as the proximity of intermolecular contacts in a  
37 molecular crystal. The function  $d_{norm}$ , which is normalized contact distance, takes into account the  
38 van der Waals radius of the appropriate atom internal or external to the surface.<sup>46</sup>  
39  
40  
41  
42  
43  
44

45 The red colour visualised in the Hirshfeld surface analysis represents a close contact and the value  
46 of the  $d_{norm}$  would be negative indicating the sum of  $d_i$  and  $d_e$  is shorter than the sum of the van der  
47 Waals radii of the atoms. The blue colour denotes a contact longer than the van der Waals radii  
48 and the  $d_{norm}$  would be positive, whereas the white colour denotes intermolecular distance close to  
49 van der Waals contacts with  $d_{norm}$  equal to zero (Figure 5a-5d).  
50  
51  
52  
53  
54  
55  
56  
57  
58  
59  
60

1  
2  
3 Hirshfeld surfaces and 2D fingerprint plots were created from Crystal Explorer 17<sup>47</sup> program based  
4 on the CIF generated from single crystal X-ray diffraction studies.<sup>48</sup> The existence of different  
5 types of intermolecular interactions is represented by 2D fingerprint plots showing  $d_i$  versus  $d_e$ .  
6

7  
8 The Hirshfeld surfaces for the prepared ILs were analysed to quantify the various intermolecular  
9 interactions, and their associated fingerprint plots were also calculated. The quantitative measures  
10 like area, volume, globularity and asphericity were also computed using the Hirshfeld surfaces.  
11  
12 The calculated value of globularity<sup>49</sup> for all the ILs was  $< 1.0$ , indicating that the molecular surface  
13 is not a sphere, but structured. The order of globularity for the ILs is [TMG][BEN]  $>$  [TMG][PTA]  
14  $>$  [TMG][SAL]  $>$  [TMG][CNA] (Table 3).  
15  
16

17  
18 The asphericity, which is a measure of anisotropy was also calculated and the order for the ILs is  
19 [TMG][CNA]  $>$  [TMG][PTA]  $>$  [TMG][SAL]  $>$  [TMG][BEN] (Table 3).  
20  
21

22 The fingerprint plots of the ILs showed spike of various thickness and lengths. Most importantly,  
23 in the two-dimensional fingerprint plots for the carboxylic acids, the hydrogen bond dominates  
24 and the appearance of sharp spikes pointing towards the bottom left of each plot is observed, in  
25 which case the upper spike (where  $d_e > d_i$ ) corresponds to the hydrogen-bond donor and the lower  
26 spike (where  $d_e < d_i$ ) corresponds to the hydrogen-bond acceptor<sup>48</sup>.  
27  
28

29  
30 The overall fingerprint plot for [TMG][BEN] (Figure 5a) and the corresponding plots delineated  
31 into H-H, O-H/H-O and C-H/H-C contacts are illustrated in Figure 5b–5d. Similarly the overall  
32 fingerprint plot of [TMG][SAL], [TMG][CNA] and [TMG][PTA] is illustrated in Figure 6a,  
33 Figure 7a and Figure 8a respectively. In all the ILs the non-polar H-H interaction is dominant and  
34 a considerable percentage of O-H/ H-O, C-H/H-C interactions is also seen (Table 4).  
35  
36  
37  
38  
39  
40  
41  
42  
43  
44  
45  
46  
47  
48  
49  
50  
51  
52  
53  
54  
55  
56  
57  
58  
59  
60

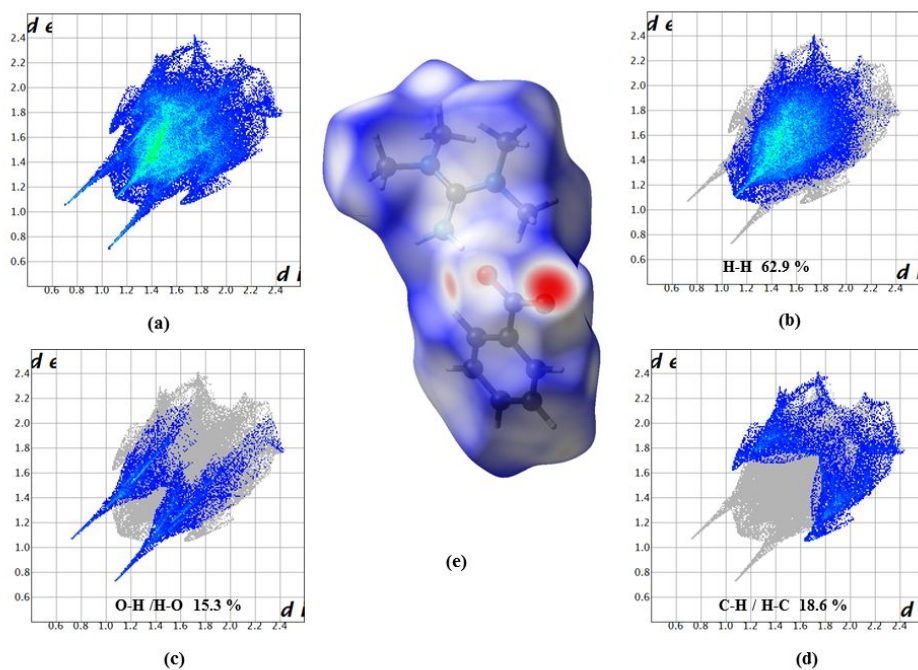


**Figure 5.** Two-dimensional fingerprint plots calculated for [TMG][BEN] (a) overall plot, (b) H-H, (c) O-H/H-O, (d) C-H/H-C contacts and (e) Hirshfeld surface mapped over  $d_{norm}$  for [TMG][BEN] with Isovalue 0.5.

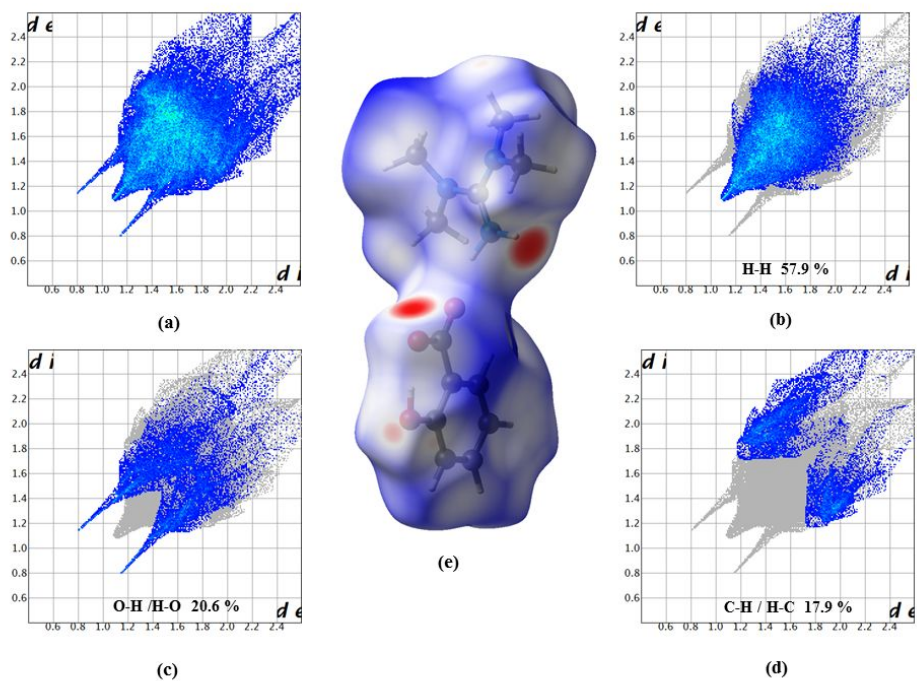


**Figure 6.** Two-dimensional fingerprint plots calculated for [TMG][SAL] (a) overall plot, (b) H-H, (c) O-H/H-O, (d) C-H/H-C contacts and (e) Hirshfeld surface mapped over  $d_{norm}$  for [TMG][SAL] with Isovalue 0.5.

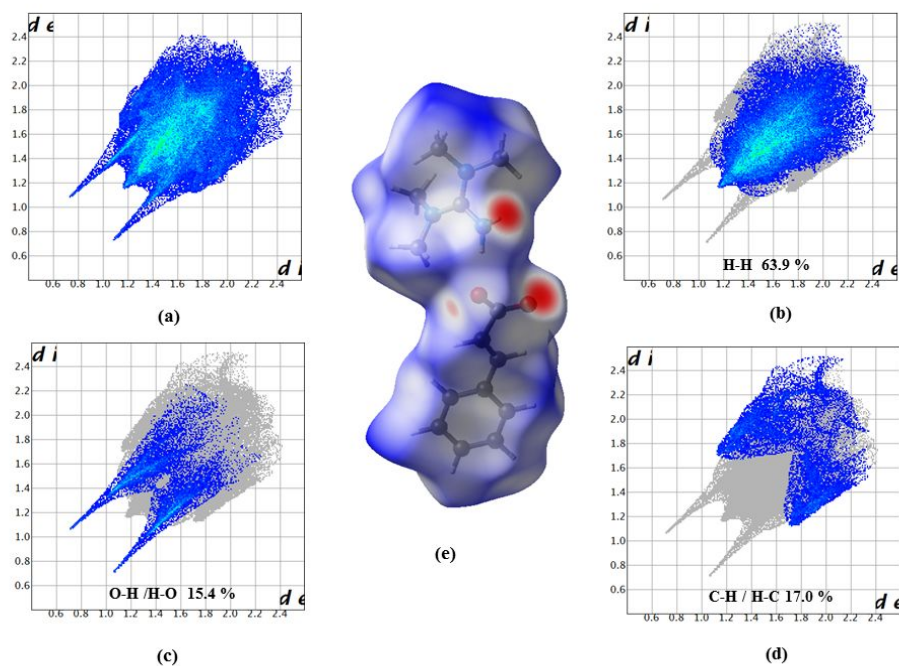


**Figure 7.** Two-dimensional fingerprint plots calculated for [TMG][CNA] (a) overall plot, (b) H-H, (c) O-H/H-O, (d) C-H/H-C contacts and (e) Hirshfeld surface mapped over  $d_{norm}$  for [TMG][CNA] with Isovalue 0.5.

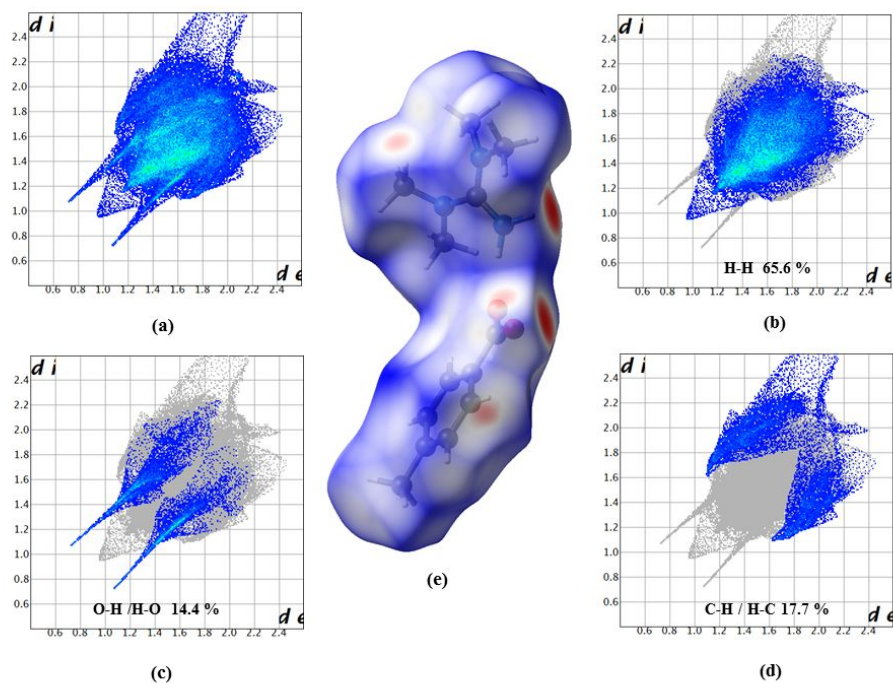


**Figure 8.** Two-dimensional fingerprint plots calculated for [TMG][PTA] (a) overall plot, (b) H-H, (c) O-H/H-O, (d) C-H/H-C contacts and (e) Hirshfeld surface mapped over  $d_{norm}$  for [TMG][PTA] with Isovalue 0.5.

#### 4. Computational details

The density functional theory (DFT) calculation has been a very useful tool to understand the fundamental vibrations and the electronic structure of a compound. The computational calculations were performed using Gaussian 09 Program<sup>50</sup> and the output files are visualized using Gauss View software<sup>51</sup>. The optimized structure, vibrational spectra, structural characteristics, energy, stability and the thermodynamic properties of the four ILs were determined with B3LYP (Becke's three parameter hybrid model using Lee-Yang-Parr correlation functional)<sup>52,53</sup> method and by using basis set 6-311G ++(d,p). Furthermore, HOMO and LUMO energy values and the energy gap were calculated for the four ILs by the same method.

##### 4.1 Molecular geometry

The optimized molecular structure of the four ILs was obtained from Gaussian 09<sup>50</sup> and Gauss view programs<sup>51</sup> using B3LYP/6311-G++(d,p) method. The molecular structures of the optimized four ILs are shown in Figure 9. It is found that most of the optimized bond lengths obtained from theoretical values are slightly larger than the experimental values as theoretical calculations belong to isolated molecules in gaseous phase while the experimental results belong to molecules in solid state and liquid state. The DFT results show a fairly good agreement with the experimental data obtained from crystallographic studies.

##### 4.2 Thermodynamic properties

Quantum mechanics, spectroscopy and thermodynamics are linked to partition function, which is an important parameter in thermodynamics. Partition functions such as, translational partition function, rotational partition function, vibrational partition function, and electronic partition function are used to calculate the heat capacity, entropy, equilibrium and rate constant. The total energy of a molecule contributes to sum of translational, rotational, vibrational and electronic energies i.e.,  $E=E_t+E_r+E_v+E_e$ . The thermodynamic parameters such as zero point vibrational energies, specific heat, rotational constants, the entropy and dipole moment values of four ILs were calculated using B3LYP/6-311++G(d,p) basis set at room temperature (298.15 K) and one atmospheric pressure. According to the obtained data, several interesting results are deduced (Table 5).

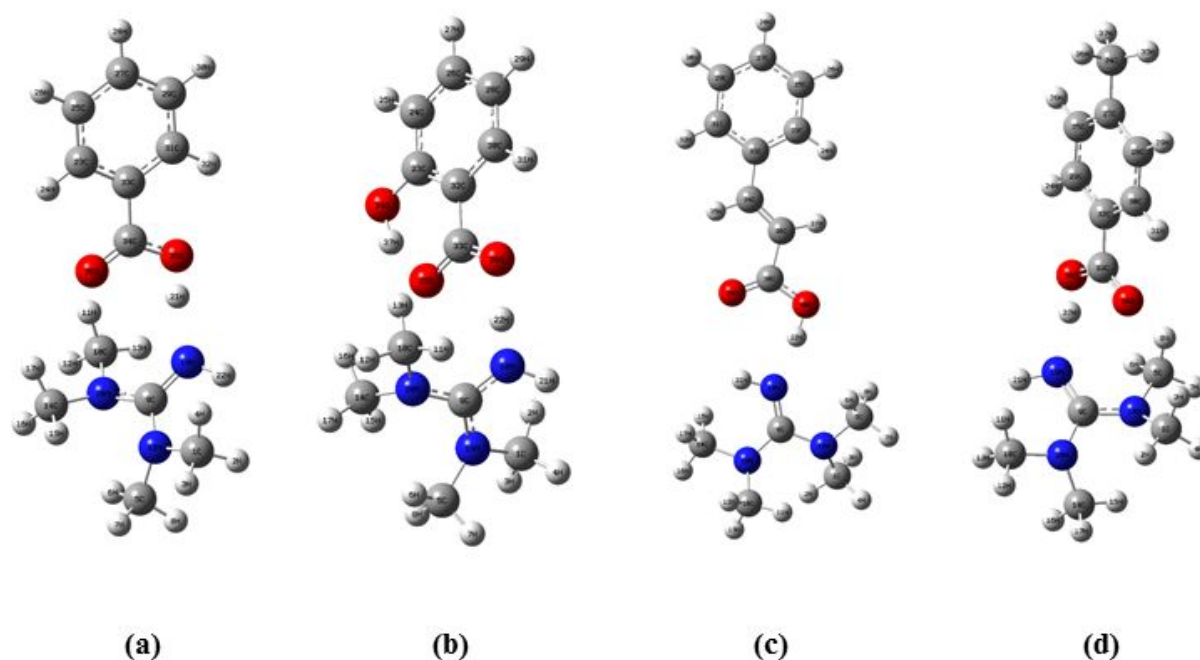


**Figure 9.** Optimized geometries of the four ILs (a) [TMG][BEN], (b) [TMG][SAL], (c) [TMG][CNA] and (d) [TMG][PTA] as obtained from DFT/B3LYP calculations with Gaussian 6-311++(d,p) basis set.

First, there is a reasonable correlation between the dipole moment of these ILs and their corresponding energy values. In other words, [TMG][SAL] has a higher dipole moment (9.152 Debye) than those of the other ILs. Strikingly, a significant declining trend of the HOMO and LUMO energy levels was evident. These are vital in predicting the reactive properties of a chemical reaction.

The thermodynamic functions such as heat capacity, entropy and enthalpy changes at different temperatures (100 K -1000 K) were also obtained from the harmonic frequency calculations based on the vibrational analysis using B3LYP method and 6-311++G(d, p) basis set for the four ILs and are listed in Table 6.

The molecular vibrational intensities of the molecule increases with the increase in temperature and this is observed in all the cases of the compound studied with temperature ranging from 100 to 1000 K. The correlation equations between heat capacity, entropy, enthalpy, Gibb's free energy and temperature for each ILs were calculated using a second order polynomial function. The

corresponding regression factor ( $R^2$ ) for the thermodynamic properties was found to be close to 0.999 for all ILs. The corresponding fitting equations for all the ILs are given in supporting information (S1), values are listed in Table 6 and the correlation graphs are shown in Figure 10a-10d. The thermodynamic properties calculated from the above equation will be useful to estimate the spontaneity of the reaction, if these ILs were used in a reaction. Further, these are important in evaluating ILs in thermal storage, heat transfer applications and heat capacity measurements.

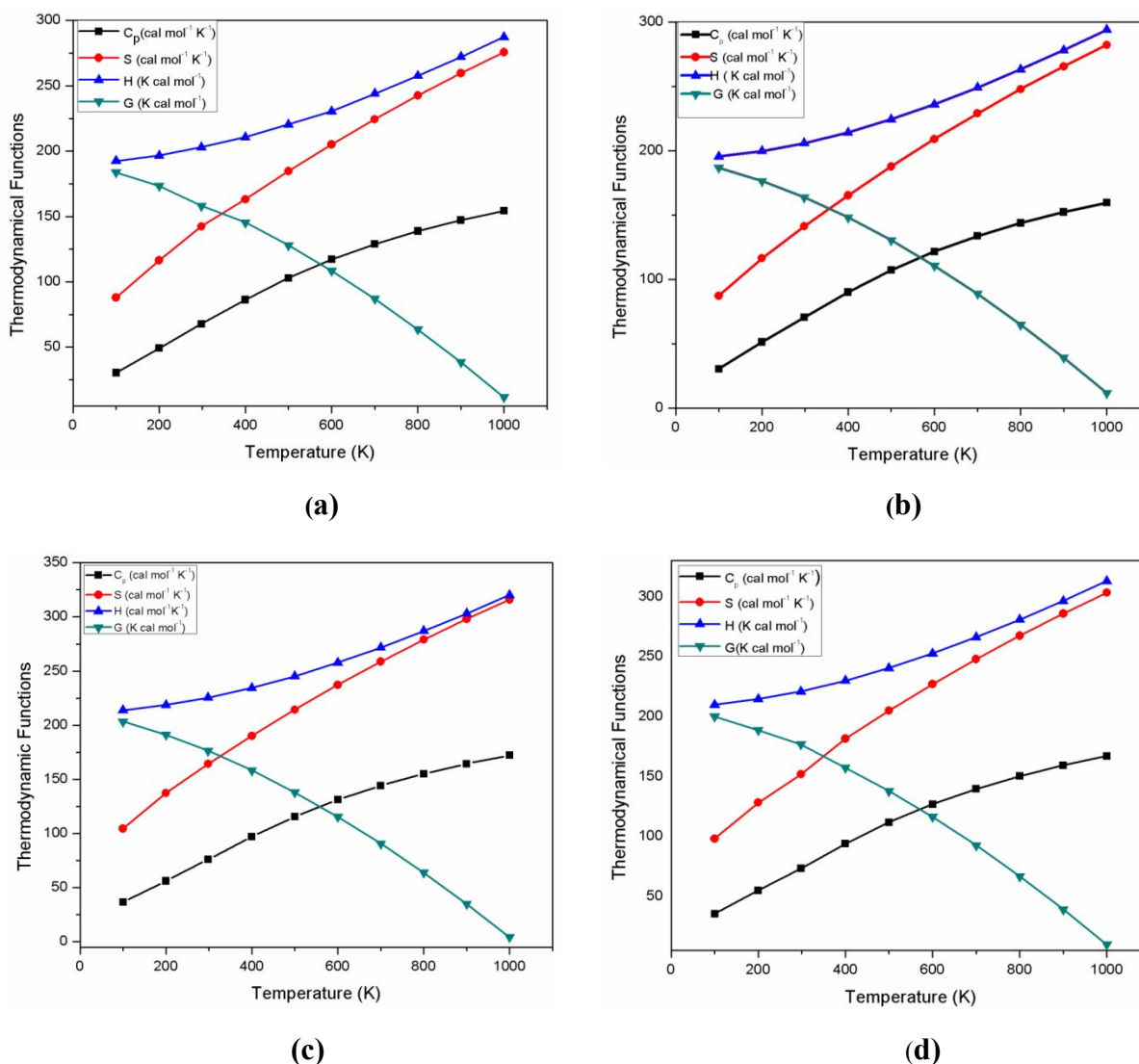


**Figure 10.** Variation in thermodynamic parameters with temperature for (a) [TMG][BEN], (b) [TMG][SAL], (c) [TMG][CNA] and (d) [TMG][PTA].

### 4.3. HOMO-LUMO analysis

The chemical reactivity can be understood by the electronic absorption transition from the ground state to the excited state and is mainly described by one electron excitation from the highest occupied molecular orbital (HOMO) to the lowest unoccupied molecular orbital (LUMO). The HOMO-LUMO energy gap calculated by computational study reflects on the chemical reactivity of the molecule, where LUMO represents the electron acceptor and HOMO represents the ability to donate an electron. The HOMO-LUMO energy gap reveals whether charge transfer interactions are taking place between the cation and anion of the molecule and to understand the ionic interaction between the cation and anions of the ILs. Generally, LUMO energies correspond to cations (electrophile), which receive the electrons from donors and HOMO energies correspond to the anions (nucleophile), which donate the electrons to the acceptors. The energy of the HOMO is related directly to the ionization potential and that of the LUMO to electron affinity. From the HOMO-LUMO energy gap, the molecular properties like chemical hardness, reactivity and stability could be predicted. The greater the energy gap, harder the molecule will be, less reactive and more stable.

The other important parameters such as Chemical hardness ( $\eta$ ), electronegativity ( $\chi$ ), chemical potential ( $\mu$ ) and electrophilicity index ( $\psi$ ) were also calculated from the ionization potential ( $-E_{\text{HOMO}}$ ) and electron affinity ( $-E_{\text{LUMO}}$ ) values for the four ILs.

$$\text{Chemical hardness } (\eta) = (E_{\text{LUMO}} - E_{\text{HOMO}}) / 2 \quad (1)$$

$$\text{Electronic chemical potential } (\mu) = (E_{\text{HOMO}} + E_{\text{LUMO}}) / 2 \quad (2)$$

$$\text{Electronegativity } (\chi) = - (E_{\text{HOMO}} + E_{\text{LUMO}}) / 2 \quad (3)$$

$$\text{Electrophilicity index } (\psi) = \mu^2 / 2\eta \quad (4)$$

From the optimized geometry, the HOMO and LUMO region levels were found to spread over the entire anion molecule and the charge transfer interface between the cation and anion is calculated by the energy gap between the HOMO-LUMO. The energy levels of the HOMO, LUMO, LUMO + 1 and HOMO - 1 orbitals were computed at B3LYP/6-311G++(d,p) level for the four ILs and are represented in Figure 11a-11d. The calculated values are given in Table 7. The surface of the frontier orbitals was drawn to understand the bonding scheme of the four ILs. The positive is represented by red and the negative by green colours.

Table 7 shows the HOMO and LUMO energy gap of the studied ILs. The observed HOMO-LUMO energy gap for [TMG][SAL] is the least value compared to the energy levels of other ILs. Hence, the salicylate anion has more ionic interactions with cation when compared to the other cation anion interactions.

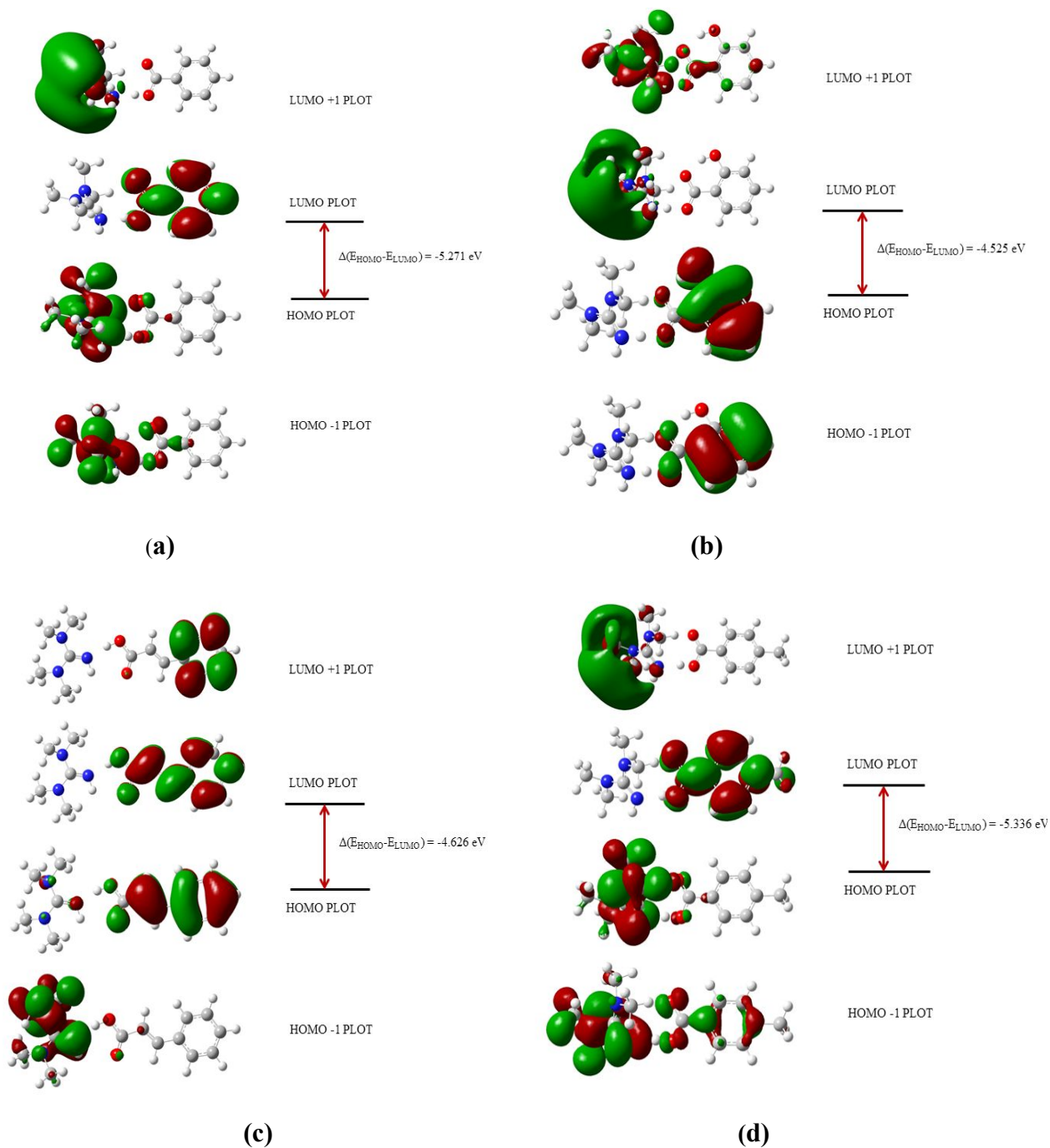


**Figure 11.** Frontier molecular orbitals of (a) [TMG][BEN], (b) [TMG][SAL], (c) [TMG][CNA] and (d) [TMG][PTA]

## 5. Thermal analysis

The thermal stability of ILs is found to depend on the anion type, chain length and allyl-functionalization<sup>54</sup>. Anion type in ILs plays a major role on the thermal stability than the cation type. The thermal stability of ILs increases with shorter chain length and the allyl-functionalization decreased the thermal stability<sup>54</sup>. The dynamic decomposition experiment of four ILs was performed under nitrogen atmosphere using TA Instruments (Q 500 Hi-Res TGA). The important information on thermal stability is the decomposition onset temperature ( $T_{d-onset}$ ), which was arrived at from the thermogravimetric data. The  $T_{d-onset}$  temperatures of [TMG][BEN], [TMG][SAL], [TMG][CNA] and [TMG][PTA] are 210.2 °C, 131.3 °C, 102.4 °C and 115.6 °C, respectively (Figure 12). The  $T_{onset}$  temperatures for 5% decomposition of [TMG][BEN], [TMG][SAL], [TMG][CNA] and [TMG][PTA] are 121.6 °C, 160.9 °C, 87.1 °C and 144.4 °C, respectively. The DSC analysis, performed on TA instruments Q200 MSDC showed that only [TMG][BEN] exhibited crystallization and melting transitions but the other three ILs did not exhibit crystallization or melting transitions, instead glass transition ( $T_g$ ) was observed. The  $T_g$  temperature of [TMG][SAL], [TMG][CNA] and [TMG][PTA] are -7.90 °C, -22.13 °C and -18.74 °C, respectively at 5 °C/min heating. [TMG][BEN] showed melting at 95.26 °C and crystallization below room temperature (Figures S5-S9). ILs usually tend to form glasses easily at low temperature and so,  $T_g$  values determine the lower limit of operating range, where the IL is liquid, and  $T_{d-onset}$  can be regarded as the upper operating range, where ILs do not evaporate.

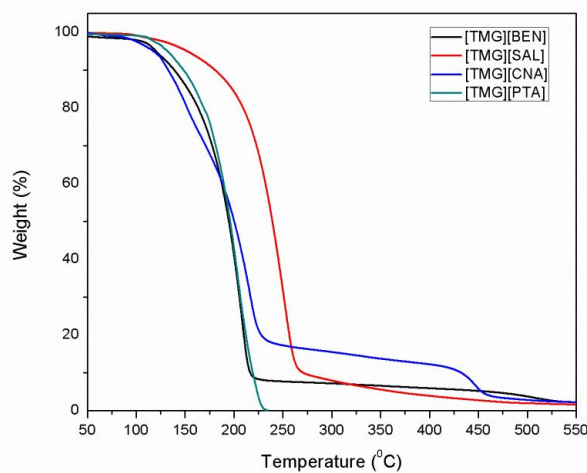


**Figure 12.** TGA analysis of [TMG][BEN], [TMG][SAL],[TMG][CNA] and [TMG][PTA]

## 6. Vibrational spectral analysis

Theoretical calculations were performed using density functional theory B3LYP with 6-31G++(d,p) basis set. Since the DFT potentials overestimate the vibrational wavenumbers, the discrepancies caused are corrected by scaling the calculated wavenumbers with the proper factor directly<sup>55</sup>. Here, we have adopted the scaling factor of 0.978 for B3LYP method. The optimized structural parameter was calculated with the above said basis sets and the values are compared with the experimental values of all ILs ornately. The FTIR spectra of the ILs were recorded in the region 4000–400  $\text{cm}^{-1}$  using JASCO 4100 model FTIR spectrometer equipped with MCT detector, a KBr beam splitter and High-Intensity ceramic source.

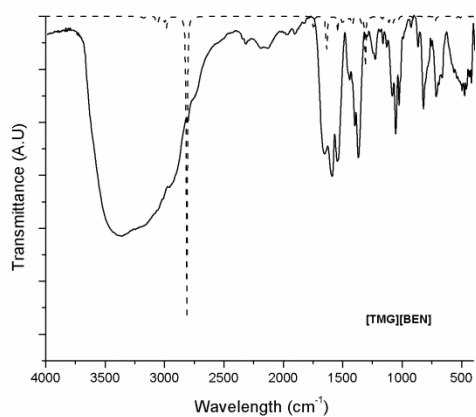
The infrared stretching vibration frequencies of N-H and C=N in TMG as reported by Anderson and Hammer<sup>56</sup> are 3311 and 1594  $\text{cm}^{-1}$ , respectively and these are observed in all the three ILs. During the protonation of the =NH group in TMG to  $-\text{NH}_2^+$  a prominent band was observed from 2700 to 2250  $\text{cm}^{-1}$ , which may be due to the formation of triaminocarbonium ion. Three types of vibrations (stretching, in-plane bending and out-of-plane bending vibrations) of O–H group (anion) were seen. The synthesized ILs were moisture sensitive and so the O–H group vibrations are likely to be present as a broad peak, which are generally observed in the region around 3500  $\text{cm}^{-1}$ . The recorded spectrum of [TMG][BEN] shows the vibrations of C=O (COO-) asymmetric and symmetric stretching at 1666  $\text{cm}^{-1}$  and 1381  $\text{cm}^{-1}$ , respectively (Figure 13a). Further, C=C (phenolic) multiple peaks appear at 1551  $\text{cm}^{-1}$ . The C-C stretching peaks were observed at 1551-1407  $\text{cm}^{-1}$ . The COO-(C-O) stretching peak appeared at 1235  $\text{cm}^{-1}$ . The vibrational peaks appearing in the region 760-670  $\text{cm}^{-1}$  were attributed to =C-H bending. The calculated vibrational frequencies by B3LYP/6-311G(d,p) method for [TMG][BEN] shows a dominant O-H vibration at 2813 $\text{cm}^{-1}$ . The asymmetric and symmetric stretching frequencies were observed at 1641  $\text{cm}^{-1}$  and 1346  $\text{cm}^{-1}$ , respectively.

The recorded spectrum of [TMG][SAL] showed vibrations of C=O (COO-) asymmetric and symmetric stretching at 1652-1670  $\text{cm}^{-1}$  and 1386  $\text{cm}^{-1}$ , respectively (Figure 13b). Further, C=C (phenolic) multiple peaks appeared at 1558-1610  $\text{cm}^{-1}$ . The C-C stretching peaks were observed at 1444-1503  $\text{cm}^{-1}$ . The O-H (phenolic) bending peak appeared at 1324  $\text{cm}^{-1}$  and the O-H stretching was observed around 3100  $\text{cm}^{-1}$ . The COO- (C-O) stretching and C-OH (phenolic) stretching peaks appeared at 1296  $\text{cm}^{-1}$  and 1156-1248  $\text{cm}^{-1}$ , respectively. The vibrational peaks appearing in the region 759-669  $\text{cm}^{-1}$  were attributed to =C-H bending. The calculated vibrational

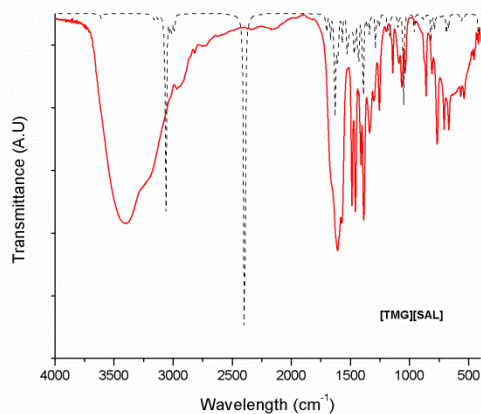
1  
2  
3 frequencies by B3LYP/6-311G(d,p) method for [TMG][SAL] showed a dominant N-H vibration  
4 at  $2386\text{cm}^{-1}$  and O-H stretching at  $3052\text{cm}^{-1}$ . The asymmetric and symmetric stretching frequency  
5 was observed at  $1617\text{cm}^{-1}$  and  $1383\text{cm}^{-1}$  respectively.  
6  
7

8 The IR spectrum of [TMG][CNA] has its own characteristic peaks corresponding to the functional  
9 groups  $-\text{COOH}$  and  $\text{C}=\text{C}$  that are present in the cinnamic acid.  $\text{C}=\text{O}$  double bond stretching  
10 frequency was observed at  $1642\text{cm}^{-1}$  due to the conjugation effect (Figure 13c). Further, the  
11  $-\text{COOH}$  functional group has a broad band O-H stretching from  $3100\text{cm}^{-1}$  to  $2800\text{cm}^{-1}$  and a C-  
12 O stretching at  $1240\text{cm}^{-1} \sim 1380\text{cm}^{-1}$ . The two bands at  $1412\text{cm}^{-1}$  and  $1642\text{cm}^{-1}$  are assigned to  
13 the aromatic  $\text{C}=\text{C}$  double bond in cinnamic acid. The aromatic  $\text{C}=\text{C}$  double bond was actually  
14 observed between  $1700\text{cm}^{-1}$  and  $1500\text{cm}^{-1}$ , but they shifted to lower wavenumber due to the  
15 conjugation effect of benzene ring. In addition, the band of aliphatic  $\text{C}=\text{C}$  double bond is  
16 overlapped by the aromatic  $\text{C}=\text{C}$  double bond stretch, which is actually present between  
17  $1642\text{cm}^{-1}$  to  $1616\text{cm}^{-1}$  with a single peak (aromatic has two peaks). The calculated vibrational  
18 frequencies by B3LYP/6-311G(d,p) method for [TMG][CNA] showed a dominant N-H vibration  
19 at  $2879\text{cm}^{-1}$ . The asymmetric and symmetric stretching frequencies were observed at around  
20  $1617\text{cm}^{-1}$  and  $1383\text{cm}^{-1}$ , respectively. The aromatic double bond vibration frequency in the cinnamic  
21 acid was found at  $1639\text{cm}^{-1}$  and the stretching frequency of aliphatic  $\text{C}=\text{C}$  double bond was  
22 observed at  $1683\text{cm}^{-1}$ .  
23  
24  
25  
26  
27  
28  
29  
30  
31  
32  
33

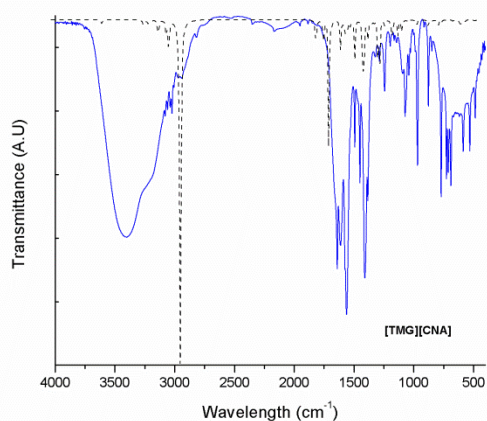
34 The IR spectrum of [TMG][PTA] showed an aromatic C-H stretching peak at  $3033\text{cm}^{-1}$ . The  
35  $\text{C}=\text{O}$  stretching (carboxylic acid) peak appeared at  $1655\text{cm}^{-1}$ . The peak due to aromatic ring  
36 stretching appeared at  $1547\text{cm}^{-1}$ . The  $\text{CH}_3$  bending peak appeared at  $1453\text{cm}^{-1}$  and C-C stretching  
37 peak was found at  $1402\text{cm}^{-1}$  (Figure 13d). Similarly C-O stretching (carboxylic acid) peak  
38 appeared at  $1381\text{cm}^{-1}$  and C-OH stretching peak appeared at  $1287\text{cm}^{-1}$ . The O-H bending peak  
39 was found at  $916\text{cm}^{-1}$ .  
40  
41  
42  
43  
44  
45  
46  
47  
48  
49  
50  
51  
52  
53  
54  
55  
56  
57  
58  
59  
60



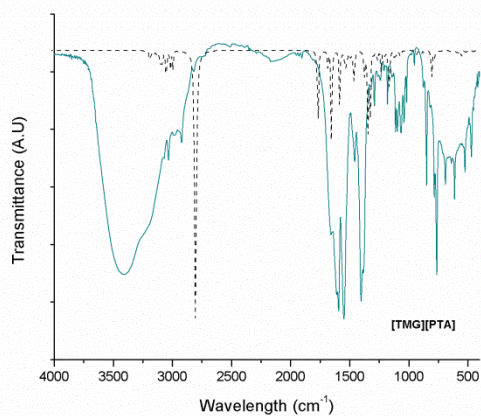
(a)



(b)



(c)



(d)

**Figure 13.** Calculated IR spectra using B3LYP/6-31G++(d,p) basis set (---- dashed line) and Experimental FTIR absorption spectra (—continuous line) of compounds (a) [TMG][BEN], (b) [TMG][SAL], (c) [TMG][CNA] and (d) [TMG][PTA].

## 7. Conclusions

Four ILs, [TMG][BEN], [TMG][SAL], [TMG][CNA] and [TMG][PTA] were synthesized and their structures were determined by crystallographic technique to understand the intermolecular interaction among the cations and anions. It is interesting to note that N-H...O hydrogen bonding plays an important role in crystal packing of molecule and in crystal structures of the ILs.

The structural insights of the ionic liquids, to quantify the intermolecular interactions in the molecular crystals are explored and visualized by Hirshfeld surface analysis and by associated fingerprint plots generated from the  $d_{norm}$  surface. Hirshfeld surface analysis showed a clear dominance of H...H, O...H and C...H interactions.

The thermal properties of the ILs were evaluated by TGA and DSC techniques to establish the thermal stability, weight loss and glass transition temperature giving a close accordance with the structure.

Density functional calculation provided valuable information on the geometry and the electronic structure of the ILs. The FT-IR spectra were recorded and the vibrational frequencies were explained by DFT- B3LYP method with 6-311G++(d,p) basis set for the four ILs. The difference between the observed and calculated wavenumbers was very small for most of the fundamentals. Furthermore, the thermodynamic properties, such as heat capacity, entropy, enthalpy and Gibb's free energy for the ILs were calculated theoretically. It can be observed that the molecular vibrational intensity increases with temperature and thereby the thermodynamic function also increases with temperature ranging from 100 to 1000 K. The frontier molecular orbital of ILs and excitation energies of surfaces of molecular orbitals from HOMO-1 and HOMO to LUMO, LUMO+1 were calculated using DFT-B3LYP 6-311G++(d,p).

## Supporting Information

The Supporting Information is available free of charge on the ACS Publications website.  $^1\text{H}$  and  $^{13}\text{C}$  NMR spectra, DSC heating and cooling curves, water content, CCDC numbers for X-ray crystallographic files, and the second order polynomial correlation equations between thermodynamic parameters and temperature for studied ionic liquids are provided in supporting information.

### Acknowledgements

Authors are thankful to IIT Madras for financial support through Institute Research and Development Award (IRDA): CHY/15-16/833/RFIR/RAME and Dr. A. Narayanan, IIT Madras for thermal analysis measurements of few samples.

**Table 1.** Crystal data and details of the structure determination of [TMG][BEN], [TMG][SAL], [TMG][CNA] and [TMG][PTA]

Identification code	[TMG][BEN]	[TMG][SAL]	[TMG][CNA]	[TMG][PTA]
Empirical formula	C <sub>12</sub> H <sub>19</sub> N <sub>3</sub> O <sub>2</sub>	C <sub>24</sub> H <sub>38</sub> N <sub>6</sub> O <sub>6</sub>	C <sub>14</sub> H <sub>21</sub> N <sub>3</sub> O <sub>2</sub>	C <sub>13</sub> H <sub>21</sub> N <sub>3</sub> O <sub>2</sub>
Formula weight/gmol <sup>-1</sup>	237.30	506.60	263.34	251.33
Temperature/K	173(2)	173(2)	173(2)	173(2)
Wavelength/ Å	0.71073	0.71073	0.71073	0.71073
Crystal system	Orthorhombic	Monoclinic	Monoclinic	Monoclinic
Space group	P212121	C2/c	P2(1)/c	P2(1)/c
a/ Å	7.1764(3)	20.2575(12)	12.1053(16)	11.0111(4)
b/ Å	10.1869(5)	9.9330(6)	7.0086(9)	7.0841(2)
c/ Å	17.4148(8)	13.5455(8)	17.352(3)	17.7940(5)
β/°	-	103.779(3)	92.464(6)	92.806(15)
Volume/ Å <sup>3</sup>	1273.11(10)	2647.2(3)	1470.8(3)	1386.33(7)
Z	4	4	4	4
Density/ g/cm <sup>3</sup>	1.238	1.271	1.189	1.204
Absorption coefficient/ mm <sup>-1</sup>	0.086	0.093	0.081	0.083
Crystal size/mm	0.12 x 0.16 x 0.25	0.20 x 0.13 x 0.12	0.22 x 0.15 x 0.12	0.10 x 0.22 x 0.25
Theta range for data collection/ <sup>0</sup>	2.32 to 25.00	2.070 to 24.999	2.350 to 24.997	2.29 to 25.00
Limiting indices	-8<=h<=6, -9<=k<=12, -20<=l<=20	-24<=h<=24, -11<=k<=11, -14<=l<=16	-10<=h<=14, -8<=k<=6, -20<=l<=20	-13<=h<=12, -8<=k<=8, -20<=l<=21
Reflections collected / unique	5521 / 223	7410 / 2289	8529 / 2587	9378/2449
R (int)	0.0164	0.0261	0.0568	0.0246
Completeness to theta = 24.999/%	99.6	98.3	100	100.0
Absorption correction	Multi-scan	Multi-scan	Multi-scan	Multi-scan
Data / restraints / parameters	2236 / 0 / 166	2289 / 0 / 179	2587 / 0 / 184	2449/0/177
Goodness-of-fit on F <sup>2</sup>	1.061	1.040	1.002	1.055
Final R indices [I>2σ(I)]	R1 = 0.0265, wR2 = 0.0679	R1 = 0.0432, wR2 = 0.1104	R1 = 0.0506, wR2 = 0.1022	R1 = 0.0398, wR2 = 0.1045
R indices (all data)	R1 = 0.0280, wR2 = 0.0689	R1 = 0.0580, wR2 = 0.1226	R1 = 0.1082, wR2 = 0.1292	R1 = 0.0570, wR2 = 0.1169

**Table 2.** Hydrogen-bonding geometry (Å, °)

<b>[TMG][BEN]</b>				
<i>D-H...A</i>	<i>D-H</i>	<i>H...A</i>	<i>D...A</i>	<i>D-H...A</i>
N2-H1N...O1 <sup>i</sup>	0.93(2)	1.91(2)	2.823(2)	170.0(19)
N2-H1N...O2 <sup>ii</sup>	0.83(2)	1.93(2)	2.767(2)	179.0(2)
Symmetry codes : (i) 1+x, y, z; (ii) 1-x, ½+y, ½-z;				
<b>[TMG][SAL]</b>				
<i>D-H...A</i>	<i>D-H</i>	<i>H...A</i>	<i>D...A</i>	<i>D-H...A</i>
N2-H1N...O1 <sup>i</sup>	0.90(2)	1.87(2)	2.747(2)	165.7(19)
N2-H2N...O2 <sup>ii</sup>	0.88(2)	2.08(2)	2.921(2)	160.5(18)
C5-H5C...O3 <sup>iii</sup>	0.98	2.53	3.276(3)	133.0
Symmetry codes : (i) x, 1+y, z; (ii) -x, 1+y, ½-z; (iii) x, 1-y, ½+z.				
<b>[TMG][CNA]</b>				
<i>D-H...A</i>	<i>D-H</i>	<i>H...A</i>	<i>D...A</i>	<i>D-H...A</i>
N2-H1N...O1 <sup>i</sup>	0.94(3)	1.91(3)	2.837(3)	170(2)
N2-H2N...O2 <sup>ii</sup>	0.95(2)	1.85(3)	2.794(3)	171(2)
Symmetry codes : (i) 1-x, 1-y, -z; (ii) 1-x, -y, -z.				
<b>[TMG][PTA]</b>				
<i>D-H...A</i>	<i>D-H</i>	<i>H...A</i>	<i>D...A</i>	<i>D-H...A</i>
N2-H1N...O1 <sup>i</sup>	0.93(2)	1.90(2)	2.818(2)	172(2)
N2-H2N...O2 <sup>ii</sup>	0.89(2)	1.93(2)	2.821(3)	174.9(18)
Symmetry codes : (i) 1-x, -1/2+y, 1/2-z; (ii) x, 3/2-y, -1/2+z.				

**Table 3.** Quantitative measure computed for studied ILs using Hirshfeld surface analysis

<b>Anion</b>	<b>[TMG][BEN]</b>	<b>[TMG][SAL]</b>	<b>[TMG][CNA]</b>	<b>[TMG][PTA]</b>
Volume (Å <sup>3</sup> )	312.22	323.85	360.23	339.64
Area (Å <sup>2</sup> )	292.92	318.09	347.05	325.47
Globularity	0.760	0.717	0.705	0.723
Asphericity	0.105	0.308	0.424	0.353
<i>d<sub>norm</sub> min</i>	-0.657	-0.509	-0.596	-0.615
<i>d<sub>norm</sub> max</i>	1.226	1.490	1.561	1.218

**Table 4.** Relative Percentage Contributions of Interactions for Cation- Anion to overall Hirshfeld Surface Area.

Anion	[TMG][BEN]	[TMG][SAL]	[TMG][CAN]	[TMG][PTA]
H-H	62.9 %	57.9 %	63.9%	65.6 %
O-H / H-O	15.3 %	20.6 %	15.4 %	14.4 %
C-H / H-C	18.6 %	17.8 %	17.0%	17.7 %
C-O/ O-C	0.1 %	0.1 %	-	-
O-O	0.1 %	0.1 %	-	-
C-C	1.1 %	0.5 %	1.9 %	0.5 %

**Table 5.** Thermodynamic parameters of studied ILs with DFT/B3LYP method using 6-311++G(d,p) basis set.

Parameter	[TMG][BEN]	[TMG][SAL]	[TMG][CNA]	[TMG][PTA]
SCF energy E(a.u)	-783.6679	-858.9244	-861.0903	-822.7141
Zero-point Vibrational energy (kcal/mol)	192.2755	193.5246	211.2945	207.6263
Rotational constant (GHz) A	1.1014	0.8361	1.1044	1.0875
Rotational constant (GHz) B	0.1800	0.2130	0.0941	0.1447
Rotational constant (GHz) C	0.1725	0.1977	0.0880	0.1400
Thermal energy (kcal/mol)	204.065	205.385	224.745	220.203
Specific heat at constant volume $C_v$ (cal mol <sup>-1</sup> K <sup>-1</sup> )	67.432	70.551	76.000	73.309
Entropy S (cal mol <sup>-1</sup> K <sup>-1</sup> )	145.664	141.323	164.243	147.814
Dipole moment (Debye)	3.361	9.1520	3.7796	3.1038

**Table 6.** Thermodynamic functions of studied ILs.

<b>[TMG][BEN]</b>				
<b>T (K)</b>	<b><math>c_{p,m}^0</math> (cal mol<sup>-1</sup> K<sup>-1</sup>)</b>	<b><math>S_m^0</math> (cal mol<sup>-1</sup> K<sup>-1</sup>)</b>	<b><math>H_m^0</math> (Kcal mol<sup>-1</sup>)</b>	<b><math>G_m^0</math> (Kcal mol<sup>-1</sup>)</b>
100	30.39	87.90	192.47	183.69
200	49.20	116.32	196.68	173.42
298.15	67.76	150.52	203.03	158.16
400	86.27	163.13	210.61	145.36
500	103.00	184.67	220.30	127.97
600	117.14	205.10	230.33	108.47
700	128.93	224.38	244.04	86.98
800	138.82	242.52	257.64	63.63
900	147.19	259.61	272.15	38.51
1000	154.32	275.70	287.44	11.74
<b>[TMG][SAL]</b>				
<b>T (K)</b>	<b><math>c_{p,m}^0</math> (cal mol<sup>-1</sup> K<sup>-1</sup>)</b>	<b><math>S_m^0</math> (cal mol<sup>-1</sup> K<sup>-1</sup>)</b>	<b><math>H_m^0</math> (Kcal mol<sup>-1</sup>)</b>	<b><math>G_m^0</math> (Kcal mol<sup>-1</sup>)</b>
100	30.47	87.33	195.48	186.75
200	51.32	116.47	199.80	176.51
298.15	70.55	141.32	205.97	163.84
400	90.14	165.41	214.37	148.21
500	107.28	187.86	224.46	130.54
600	121.74	209.10	236.13	110.68
700	133.80	229.11	249.13	88.76
800	143.90	247.92	263.23	64.90
900	152.42	265.60	278.25	39.21
1000	159.68	282.26	294.07	11.81
<b>[TMG][CNA]</b>				
<b>T (K)</b>	<b><math>c_{p,m}^0</math> (cal mol<sup>-1</sup> K<sup>-1</sup>)</b>	<b><math>S_m^0</math> (cal mol<sup>-1</sup> K<sup>-1</sup>)</b>	<b><math>H_m^0</math> (Kcal mol<sup>-1</sup>)</b>	<b><math>G_m^0</math> (Kcal mol<sup>-1</sup>)</b>
100	36.69	104.47	213.81	203.37
200	56.14	137.39	218.67	191.19
298.15	76.00	164.24	225.33	176.37
400	97.10	190.14	234.36	158.31
500	115.64	214.29	245.22	138.08
600	131.25	237.16	257.79	115.50
700	144.24	258.70	271.78	90.69
800	155.13	278.96	286.96	63.80
900	164.34	298.01	303.15	34.94
1000	172.19	315.95	320.18	4.23
<b>[TMG][PTA]</b>				
<b>T (K)</b>	<b><math>c_{p,m}^0</math> (cal mol<sup>-1</sup> K<sup>-1</sup>)</b>	<b><math>S_m^0</math> (cal mol<sup>-1</sup> K<sup>-1</sup>)</b>	<b><math>H_m^0</math> (Kcal mol<sup>-1</sup>)</b>	<b><math>G_m^0</math> (Kcal mol<sup>-1</sup>)</b>
100	35.38	98.13	209.95	200.14
200	54.94	130.23	214.69	188.65
298.15	73.31	147.81	220.79	176.73
400	93.94	181.57	229.96	157.33
500	111.75	204.93	240.46	138.00
600	126.88	227.05	252.61	116.39
700	139.55	247.89	266.15	92.63
800	150.22	267.51	280.85	66.85
900	159.28	285.97	296.54	39.17
1000	167.02	303.37	313.06	9.69

**Table 7.** Calculated energy values and related molecular properties of [TMG][BEN], [TMG][SAL], [TMG][CNA] and [TMG][PTA]

<b>Basis Set (B3LYP/ 6-311++G(d,p))</b>	<b>[TMG][BEN]</b>	<b>[TMG][SAL]</b>	<b>[TMG][CNA]</b>	<b>[TMG][PTA]</b>
$E_{\text{HOMO}}$ (eV)	-6.418	-5.447	-6.353	-6.381
$E_{\text{LUMO}}$ (eV)	-1.147	-0.921	-1.726	-1.044
$E_{\text{HOMO}} - E_{\text{LUMO}}$ gap (eV)	-5.271	-4.525	-4.626	-5.336
Chemical Hardness ( $\eta$ )	2.635	2.262	2.313	2.338
Chemical potential ( $\mu$ )	-3.783	-3.184	-4.040	-3.713
Electronegativity ( $\chi$ )	3.783	3.184	4.040	3.713
Electrophilicity index ( $\psi$ )	2.714	2.240	3.5279	2.583

## References

- (1) Rogers, R. D.; Seddon, K. R.; Volkov, S. Green Industrial Applications of Ionic Liquids. In *Proceedings of the NATO Advanced Research Workshop on Green Industrial Applications of Ionic Liquids Heraklion, Crete, Greece*; **2003**; pp 137–156.
- (2) Peter Wasserscheid and Thomas Welton. In *Ionic Liquids in Synthesis*; Wiley-VCH Verlag GmbH & Co., **2002**; Vol. 7, pp 221–227.
- (3) Fumino, K.; Ludwig, R. Analyzing the Interaction Energies between Cation and Anion in Ionic Liquids: The Subtle Balance between Coulomb Forces and Hydrogen Bonding. *J. Mol. Liq.* **2014**, *192*, 94–102.
- (4) Abdul-Sada, A. K.; Greenway, A. M.; Hitchcock, P. B.; Mohammed, T. J.; Seddon, K. R.; Zora, J. A. Upon the Structure of Room Temperature Halogenoaluminate Ionic Liquids. *J. Chem. Soc., Chem. Commun.*, **1986**, *24*, 1753–1754.
- (5) Dymek, C. J.; Grossie, D. A.; Fratini, A. V.; Wade Adams, W. Evidence for the Presence of Hydrogen-Bonded Ion-Ion Interactions in the Molten Salt Precursor, 1-Methyl-3-Ethylimidazolium Chloride. *J. Mol. Struct.* **1989**, *213*, 25–34.
- (6) Zentel, T.; Overbeck, V.; Michalik, D.; Kühn, O.; Ludwig, R. Hydrogen Bonding in Protic Ionic Liquids: Structural Correlations, Vibrational Spectroscopy, and Rotational Dynamics of Liquid Ethylammonium Nitrate. *J. Phys. B: At. Mol. Opt.* **2018**, *51*, 1–10.
- (7) Hunt, P. A. Quantum Chemical Modeling of Hydrogen Bonding in Ionic Liquids. *Top. Curr. Chem.* **2017**, *375*, 1–22.
- (8) Desiraju, G. R. Crystal Engineering: From Molecule to Crystal. *J. Am. Chem. Soc.* **2013**, *135*, 9952–9967.
- (9) Hayes, R.; Imberti, S.; Warr, G. G.; Atkin, R. The Nature of Hydrogen Bonding in Protic Ionic Liquids. *Angew. Chem. Int. Ed.* **2013**, *52*, 4623–4627.
- (10) Roth, C.; Peppel, T.; Fumino, K.; Köckerling, M.; Ludwig, R. The Importance of

- 1  
2  
3 Hydrogen Bonds for the Structure of Ionic Liquids : Single-Crystal X-Ray Diffraction and  
4 Transmission and Attenuated Total Reflection Spectroscopy in the Terahertz Region.  
5 *Angew. Chem. Int. Ed.* **2010**, *49*, 10221–10224.  
6  
7  
8  
9 (11) Wang, X.; Vogel, C. S.; Heinemann, F. W.; Wasserscheid, P.; Meyer, K. Solid-State  
10 Structures of Double-Long-Chain Imidazolium Ionic Liquids: Influence of Anion Shape  
11 on Cation Geometry and Crystal Packing. *Cryst. Grow. Des.* **2011**, *11*, 1974–1988.  
12  
13 (12) Stappert, K.; Ünal, D.; Spielberg, E. T.; Mudring, A. V. Influence of the Counteranion on  
14 the Ability of 1-Dodecyl-3-Methyltriazolium Ionic Liquids to Form Mesophases.  
15 *Cryst. Grow. Des.* **2015**, *15*, 752–758.  
16  
17 (13) Fumino, K.; Wulf, A.; Ludwig, R. Hydrogen Bonding in Protic Ionic Liquids :  
18 Reminiscent of Water. *Angew. Chem. Int. Ed.* **2009**, No. 3, 3184–3186.  
19  
20 (14) Meng, X.; Wang, J.; Jiang, H.; Zhang, X.; Liu, S.; Hu, Y. Guanidinium-Based  
21 Dicarboxylic Acid Ionic Liquids for SO<sub>2</sub> Capture. *J. Chem. Technol. Biot.* **2017**, *92*, 767–  
22 774.  
23  
24 (15) An, D.; Wu, L.; Li, B. G.; Zhu, S. Synthesis and SO<sub>2</sub> Absorption/Desorption Properties of  
25 Poly(1,1,3,3 Tetramethylguanidine Acrylate). *Macromolecules* **2007**, *40*, 3388–3393.  
26  
27 (16) Carmen, F.; Weber, H. K.; Roder, T.; Sixta, H.; Laus, G.; Schottenberger, H. No Matter of  
28 Course: Ionic Liquids as SO<sub>2</sub>-Selective Gas Absorbers. *Lenzinger Berichte* **2013**, *91*, 30–  
29 43.  
30  
31 (17) Shang, Y.; Li, H.; Zhang, S.; Xu, H.; Wang, Z.; Zhang, L.; Zhang, J. Guanidinium-Based  
32 Ionic Liquids for Sulfur Dioxide Sorption. *Chem. Eng. J.* **2011**, *175*, 324–329.  
33  
34 (18) Mai, N. L.; Koo, Y. Production of Biofuels and Chemicals with Ionic Liquids. In *Springer*  
35 *Book Series*; 2014; Vol. 1, pp 257–273.  
36  
37 (19) Porwal, J.; Kumar, S.; Kaul, S.; Jain, S. L. Guanidine Based Task Specific Ionic Liquids  
38 for the Synthesis of Biolubricant Range Esters under Solvent-Free Condition. *RSC Adv.*  
39 **2016**, *6*, 93640–93644.  
40  
41  
42  
43  
44  
45  
46  
47  
48  
49  
50  
51  
52  
53  
54  
55  
56  
57  
58  
59  
60

- 1  
2  
3 (20) Zhu, A.; Jiang, T.; Han, B.; Huang, J.; Zhang, J.; Ma, X. Study on Guanidine-Based Task-  
4 Specific Ionic Liquids as Catalysts for Direct Aldol Reactions without Solvent. *New J.*  
5 *Chem.* **2006**, *30*, 736-740.  
6  
7  
8  
9 (21) Gao, H.; Han, B.; Li, J.; Jiang, T.; Liu, Z.; Wu, W.; Chang, Y.; Zhang, J. Preparation of  
10 Room-Temperature Ionic Liquids by Neutralization of 1,1,3,3-Tetramethylguanidine with  
11 Acids and Their Use as Media for Mannich Reaction. *Synthetic Commun.* **2004**, *34*, 3083–  
12 3089.  
13  
14  
15  
16 (22) Zhigang Lei, Chengna Dai, and B. C.; Lei, Z.; Dai, C.; Chen, B.; Zhigang Lei, Chengna  
17 Dai, and B. C. Gas Solubility in Ionic Liquids. *Chem. Rev.* **2014**, *114*, 1289–1326.  
18  
19  
20 (23) Lei, X.; Xu, Y.; Zhu, L.; Wang, X. Highly Efficient and Reversible CO<sub>2</sub> Capture through  
21 1,1,3,3-Tetramethylguanidinium Imidazole Ionic Liquid. *RSC Adv.* **2014**, *4*, 7052–7057.  
22  
23  
24 (24) Mudring, A. V. Solidification of Ionic Liquids: Theory and Techniques. *Aust. J. Chem.*  
25 **2010**, *63*, 544–564.  
26  
27  
28 (25) Boese, R. Special Issue on in Situ Crystallization. *Z. Krist.- Cryst. Mater.* **2014**, *229*, 595–  
29 601.  
30  
31  
32  
33 (26) Choudhury, A. R.; Winterton, N.; Steiner, A.; I.Copper, A.; Johnson, K. A. In Situ  
34 Crystallization of Low Melting Ionic Liquids. *J. Am. Chem. Soc.* **2005**, *127*, 16792–  
35 16793.  
36  
37  
38 (27) Chopra, D.; Row, T. N. G. In Situ Cryocrystallization : Pathways to Study Intermolecular  
39 Interactions. *J. Indinan I. Sci.* **2007**, *87*, 167–211.  
40  
41  
42  
43 (28) Berg, R. W.; Riisager, A.; Fehrmann, R. Formation of an Ion-Pair Molecule with a Single  
44 NH<sup>+</sup>... Cl<sup>-</sup> Hydrogen Bond: Raman Spectra of 1,1,3,3-Tetramethylguanidinium Chloride  
45 in the Solid State, in Solution, and in the Vapor Phase. *J. Phys. Chem. A* **2008**, *112*, 8585–  
46 8592.  
47  
48  
49  
50 (29) Berg, R. W.; Riisager, A.; Van Buu, O. N.; Kristensen, S. B.; Fehrmann, R.; Harris, P.;  
51 Brunetti, A. C. X-Ray Crystal Structure, Raman Spectroscopy, and Ab Initio Density  
52 Functional Theory Calculations on 1,1,3,3-Tetramethylguanidinium Bromide. *J. Phys.*  
53  
54  
55  
56  
57  
58  
59  
60

- Chem. A* **2010**, *114*, 13175–13181.
- (30) Ebrahimi, M.; Hosseinkhani, S.; Heydari, A.; Khavari-Nejad, R. A.; Akbari, J. Improvement of Thermostability and Activity of Firefly Luciferase through [TMG][Ac] Ionic Liquid Mediator. *Appl. Biochem. Biotech.* **2012**, *168*, 604–615.
- (31) Berg, R. W.; Riisager, A.; Van Buu, O. N.; Fehrmann, R.; Harris, P.; Tomaszowska, A. A.; Seddon, K. R. Crystal Structure, Vibrational Spectroscopy and Ab Initio Density Functional Theory Calculations on the Ionic Liquid Forming 1,1,3,3-Tetramethylguanidinium Bis{(Trifluoromethyl)Sulfonyl}amide. *J. Phys. Chem. B* **2009**, *113*, 8878–8886.
- (32) Criado, A.; Diáñez, M. J.; Pérez-Garrido, S.; Fernandes, I. M. L.; Belsley, M.; De Matos Gomes, E. 1,1,3,3-Tetramethylguanidinium Dihydrogenorthophosphate. *Acta Crystallogr. C* **2000**, *56*, 888–889.
- (33) Vitorino, J.; Agapito, F.; Piedade, M. F. M.; Bernardes, C. E. S.; Diogo, H. P.; Leal, J. P.; Minas Da Piedade, M. E. Thermochemistry of 1,1,3,3-Tetramethylguanidine and 1,1,3,3-Tetramethylguanidinium Nitrate. *J. Chem. Thermodyn.* **2014**, *77*, 179–189.
- (34) Singh, A. P.; Gardas, R. L.; Senapati, S. Divergent Trend in Density versus Viscosity of Ionic Liquid/Water Mixtures: A Molecular View from Guanidinium Ionic Liquids. *Phys. Chem. Chem. Phys.* **2015**, *17*, 25037–25048.
- (35) Dong, K.; Zhang, S.; Wang, J. Understanding the Hydrogen Bonds in Ionic Liquids and Their Roles in Properties and Reactions. *Chem. Commun.* **2016**, *52*, 6744–6764.
- (36) Xu, W.; Cooper, E. I.; Angell, C. A. Ionic Liquids: Ion Mobilities, Glass Temperatures, and Fragilities. *J. Phys. Chem. B* **2003**, *107*, 6170–6178.
- (37) Mihichuk, L. M.; Driver, G. W.; Johnson, K. E. Bronsted Acidity and the Medium: Fundamentals with a Focus on Ionic Liquids. *ChemPhysChem* **2011**, *12*, 1622–1632.
- (38) Sheldrick, G. M. A Short History of SHELX. *Acta Crystallogr. A* **2008**, *A64*, 112–122.
- (39) Sheldrick, G. M. Crystal Structure Refinement with SHELXL. *Acta Crystallogr. C* **2015**,

- 1  
2  
3 71, 3–8.  
4  
5  
6 (40) Farrugia, L. J. WinGX and ORTEP for Windows: An Update. *J. Appl. Crystallogr.* **2012**,  
7 45, 849–854.  
8  
9  
10 (41) Macrae, C. F.; Edgington, P. R.; McCabe, P.; Pidcock, E.; Shields, G. P.; Taylor, R.;  
11 Towler, M.; Van De Streek, J. Mercury: Visualization and Analysis of Crystal Structures.  
12 *J. Appl. Crystallogr.* **2006**, 39, 453–457.  
13  
14  
15  
16 (42) Sawinski, P. K.; Meven, M.; Englert, U.; Dronskowski, R. Single-Crystal Neutron  
17 Diffraction Study on Guanidine, CN 3 H 5. *Cryst. Grow. Des.* **2013**, 13, 1730–1735.  
18  
19  
20 (43) Steiner, T. The Hydrogen Bond in the Solid State. *Angew. Chem. Int. Ed.* **2002**, 41, 49–76.  
21  
22  
23 (44) Bernstein, J.; Davis, R. E.; Shimon, L.; Chang, N. -L. Patterns in Hydrogen Bonding:  
24 Functionality and Graph Set Analysis in Crystals. *Angew. Chem. Int. Ed.* **1995**, 34, 1555–  
25 1573.  
26  
27  
28  
29 (45) Chakraborty, S.; Desiraju, G. R. C – H ... F Hydrogen Bonds in Solid Solutions of  
30 Benzoic Acid and 4 - Fluorobenzoic Acid. *Cryst. Grow. Des.* **2018**, 18, 3607–3615.  
31  
32  
33 (46) McKinnon, J. J.; Jayatilaka, D.; Spackman, M. A. Towards Quantitative Analysis of  
34 Intermolecular Interactions with Hirshfeld Surfaces. *Chem. Commun.* **2007**, No. 37, 3814–  
35 3816.  
36  
37  
38  
39 (47) M.J.Turner; J.J.McKinnon; S.K.Wolff; D.J.Grimwood; P.R.Spackman; D.Jayatilaka;  
40 M.A.Spackman. Crystal Explorer. 2018, p Crystal Explorer 17.5, University of Western  
41 Aus.  
42  
43  
44  
45 (48) Spackman, M. A.; McKinnon, J. J. Fingerprinting Intermolecular Interactions in  
46 Molecular Crystals. *CrystEngComm* **2002**, 4, 378–392.  
47  
48  
49  
50 (49) A. Y. Meyer. The Size of Molecules. *Chem. Soc.Rev.* **1986**, 15, 449–474.  
51  
52  
53 (50) Frisch, M. J.; Trucks, G. W.; Schlegel, H. B.; Scuseria, G. E.; Robb, M. A.; Cheeseman, J.  
54 R.; Montgomery, J. A., J.; Vreven, T.; Kudin, K. N.; Burant, J. C.; et al. Gaussian 09.  
55 2016.  
56  
57  
58  
59  
60

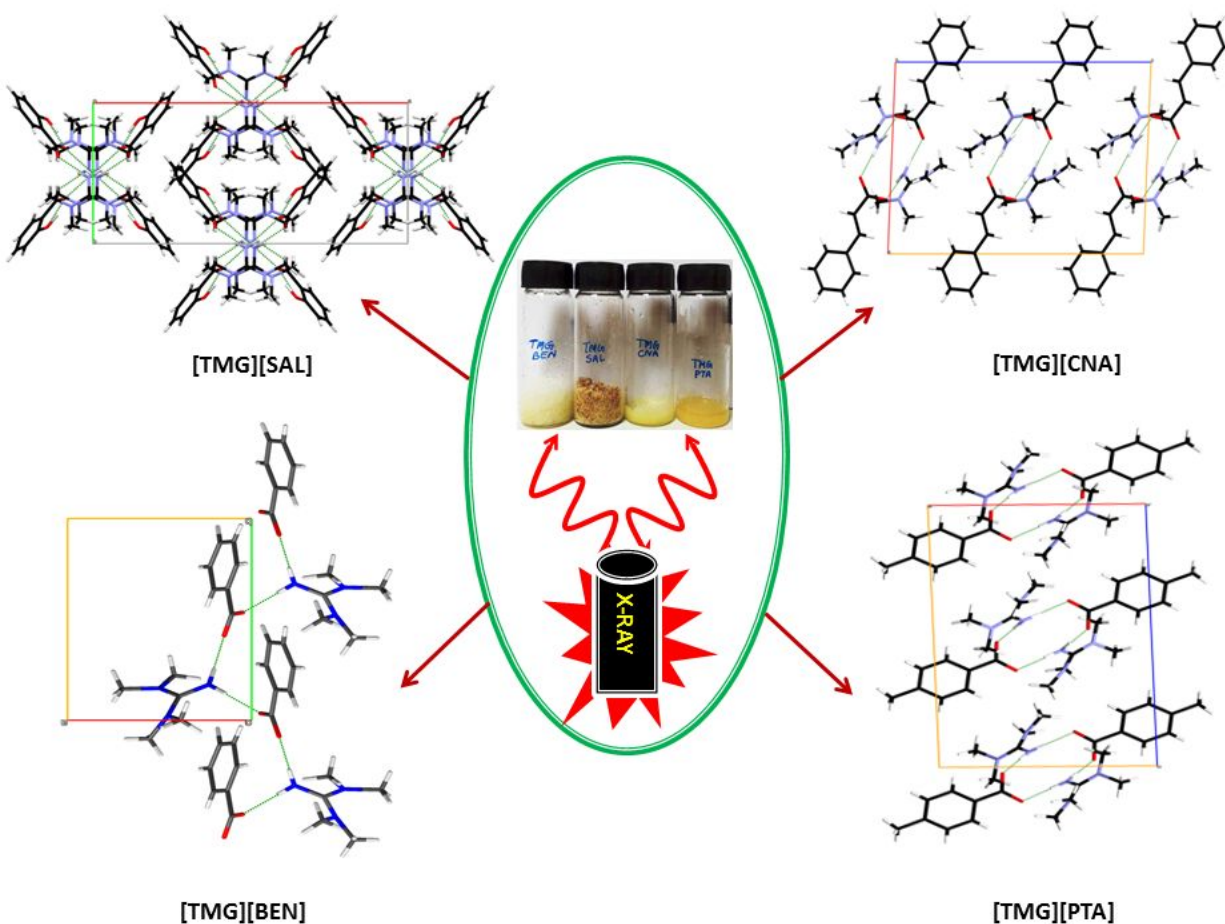
- 1  
2  
3 (51) Dennington, R.; Keith, T.; Millam, J. M. Gaussview 6.0. Semichem Inc., Shawnee  
4 Mission, KS, 2016.  
5  
6  
7 (52) Becke, A. D. Density-Functional Thermochemistry. III. The Role of Exact Exchange. *J.*  
8 *Chem. Phys.* **1993**, *98*, 5648–5652.  
9  
10  
11 (53) Lee, C.; Yang, W.; Parr, R. G. A Functional of the Electron Density. *Phys. Rev. B*  
12 **1988**, *37*, 785–789.  
13  
14  
15 (54) Cao, Y.; Mu, T. Comprehensive Investigation on the Thermal Stability of 66 Ionic Liquids  
16 by Thermogravimetric Analysis. *Ind. Eng. Chem. Res.* **2014**, *53*, 8651–8664.  
17  
18  
19 (55) Scott, A. P.; Radom, L. Harmonic Vibrational Frequencies: An Evaluation of Hartree-  
20 Fock, Møller-Plesset, Quadratic Configuration Interaction, Density Functional Theory,  
21 and Semiempirical Scale Factors. *J. Phys. Chem.* **1996**, *100*, 16502–16513.  
22  
23  
24 (56) Anderson, M. L.; Hammer, R. N. Properties of 1,1,3,3-Tetramethylguanidine as a  
25  
26  
27  
28  
29  
30  
31  
32  
33  
34  
35  
36  
37  
38  
39  
40  
41  
42  
43  
44  
45  
46  
47  
48  
49  
50  
51  
52  
53  
54  
55  
56  
57  
58  
59  
60

**For Table of Contents Use Only**

**Structural Arrangement and Computational Exploration of Guanidinium Based Ionic Liquids with Benzoic Acid Derivatives as Anion**

V. Ramkumar, Indrajit Das and Ramesh L. Gardas\*

Department of Chemistry, Indian Institute of Technology Madras, Chennai – 600036, India



*In situ* cryo-crystallisation method has been used to study the crystal structure and the intermolecular interaction among the cations and anions of 1,1,3,3-tetramethylguanidine [TMG] based ionic liquids. Results are supported with Hirshfeld surface analysis and DFT calculations.